Structural and dynamic aspects of electron transfer in proteins — highly organized natural nanostructures

A. I. Kotelnikov, E. S. Medvedev, and N. S. Goryachev*

Institute of Problems of Chemical Physics, Russian Academy of Sciences,
1 prosp. Akad. Semenova, 142432 Chernogolovka, Moscow Region, Russian Federation.
Fax: +7 (496) 522 3507. E-mail: kotel@icp.ac.ru

The review briefly outlines theoretical models developed in 1990s to describe electron transfer reactions (ETR) in proteins, as well as different variants of improvements in these models proposed by the present authors to describe ETR in reaction centers (RC) of photosynthetic bacteria with consideration of their molecular dynamics in a wide temperature range. Experimental data on electron transfer from reduced proximal heme c-559 of cytochrome to bacteriochlorophyll dimer radical cation P^+ in RC from two types of bacteria, *viz.*, native and mutant RC from *Rps. viridis* and native RC from *Rps. sulfoviridis* were analyzed within the framework of the models which take into account the quantum and classical (including diffusive) degrees of freedom responsible for reorganization of the protein globule.

Key words: electron transfer, heme-containing proteins, reaction centers, nonexponential kinetics, nonadiabatic and adiabatic approximations, combined model, matrix element, free energy, reorganization energy, protein dynamics.

Introduction

An opinion that electron transfer reactions (ETR) are key to many biochemical processes in living organisms and plants dates back to the middle of the 20th century.

At present, one can state with certainty that the existence of a living organism consisting mainly of organic molecules and water in oxygen atmosphere is only possible due to a strict separation and ordering of redox reactions in space and time. Electron transfer reactions (ETR) and related reactions involving transfer of other charged particles in biological systems are basic to energy storage and transformation, synthesis of new biomacromolecules, as well as data storage and processing. Analysis of general factors determining the rate of such reactions is important for both fundamental research and from the standpoint of design of novel, highly efficient catalysts and artificial systems for energy storage and transformation.

At the turn of 1960s, amazing examples of microscopic, supercompact recording information in biological systems were reported and the problem of using principles of living nature for the design of microcomputers with conductors 10 to 100 atoms in diameter and single integrated circuits a few thousands of Ångstrøms in size was posed.[1] Since then, five decades have passed. Particular elements in modern electronic devices became less than a biological cell and are now 45 nm in size; this is only 3 to 10 times larger than the characteristic sizes of large proteins, elements of membrane structures, or DNA molecules. With respect to the volume density of logical elements modern electronic devices seem to approach the packing density of neurons in human brain and demonstrate a much higher performance.

However, it is a rapid miniaturization of integrated circuits that allows one to predict a close limit of their improvement within the framework of traditional technologies. Further progress in electronics at the expense of miniaturization of individual elements to atomic or molecular structures 1—3 nm in size is limited by some fundamental reasons. First, as will be shown in detail below, as the distance between two conductors becomes as short as 1—2 nm, electron leakage occurs due to quantum tunneling effects. Second, heat release abruptly increases with a decrease in the cross-section of the conductor and the problem of heat sink appears.

Further miniaturization unavoidably causes the need to develop molecular electronic devices whose engineering, assembly, and fundamental principles of operation in the single-electron transfer regime are basically different from the principles used by modern electronics. Promising avenues of the development of molecular electronics can be formulated after thorough investigation of processes in living nature.

As noted above, numerous studies revealed that efficient occurrence of the most important biological processes in living organisms is due to ordered and directed electron transfer between metal-containing or organic centers in biological macromolecules.

Published in Russian in *Izvestiya Akademii Nauk. Seriya Khimicheskaya,* No. 7, pp. 1295—1318, July, 2011.

1066-5285/11/6007-1318

The authors of the early studies proposed various hypotheses on the reasons for high efficiency of electron transfer in proteins. In particular, it was assumed that, owing to their polypeptide structure and the presence of highly ordered α-helices, proteins may exhibit band-type conduction varying along different directions similarly to some organic crystals or semiconductor structures.[2,3]

Another feature of protein structures consist in their dynamic properties. The dynamics, internal mobility of the protein globule, is important for enzymatic activity of proteins. A protein should change its structure in the course of the catalytic act, thus adapting the structural features of reactants. This property is inherent in proteins, which is basic to their activity. How does it influence the rate of electron transfer?

The main advantages in experimental studies of ETR in proteins were achieved in the 1970—1990s. The reasons are as follows.

First, exact molecular structures of a large number of proteins including protein complexes of reaction centers (RC) of photosynthetic bacteria were established by X-ray analysis. This made it possible to compare the experimental data on the kinetics of electron transfer with specific structures of protein globules in which electron transfer occurred.

Second, new experimental methods of investigations of electron transfer between a chromophore covalently bound to a certain protein group and a metal-containing center in the protein structure were developed. Most often, a site a heme in hemoglobin, myoglobin, and cytochrome *c* or some other metal-containing center, *e.g.*, a copper atom in the active center of azurin. One can investigate both instantaneously "switched on" direct electron transfer from excited (most often, triplet) chromophore or the reverse electron recombination reaction from the metal-containing center to the oxidized dye. Using this approach, the position of the donor or acceptor center in the protein structure can be selectively changed to vary the electron transfer length and trajectory in the protein globule. At the same time the use of different chromophores to be excited or modification of the metal-containing center in the protein serve to change the energy characteristics of the reaction over a wide range. This approach provided a considerable increase in the number of reactions studied.[4—26]

Third, various physical methods (optical spectroscopy, IR spectroscopy, Raman spectroscopy, Mössbauer spectroscopy, various kinds of ESR spectroscopy, as well as spin, fluorescent, and phosphorescent labels) were developed and effectively used. This made it possible to measure the molecular dynamics of the polypeptide chain, iron atoms in the heme structure or the surface layers of the aqueous environment of proteins on the time scale from 10^{-11} to 10^{1} s in a wide temperature range.[27—44]

Finally, general principles and theoretical models for analysis of the available experimental data were formulated.

Numerous studies revealed that in most cases, electron transfer in biological systems involves proteins. Electrons are localized on particular (most often, metal-containing) centers in protein molecules. These centers are mainly localized near the protein surface but do not directly contact the aqueous environment.

Long-range electron transfer can follow two mechanisms.

In the first case, attachment of an electron to the metal-containing site of a protein is followed by intracellular diffusion of the protein and transfer of the attached electron to the active center of another protein by diffusion collision; here, both centers should not necessarily contact each other, a distance of 5—20 Å between them being short enough.[45]

The other case is more interesting. Detailed studies on the mechanisms governing the activity of large proteins or protein-membrane complexes showed that in different redox reactions, electrons are localized on certain metal-containing sites separated by distances ranging from 5 to 20 Å, and move in a directed manner within the protein or between proteins by successively jumping from on center to another over distances of tens and hundreds of Ångstrøms, whereas the proteins *per se* show no diffusion mobility.

The processes occurring in RC (protein complexes that execute directed transmembrane charge transfer in photosynthesis) are the most striking examples of fast and highly efficient targeted electron transfer. A reaction center is a protein comprised of three polypeptide chains and having a number of chlorophyll-type pigments[46] (Fig. 1). The total molecular weight of such a protein is more than 60 kDa and its molecule contains a few thousands of atoms. On excitation of a bacteriochlorophyll dimer (P) with a light quantum, an electron is successively transferred from its excited level to the bacteriochlorophyll monomer, pheophytin, and to the primary electron acceptor (quinone, Q) on the opposite side of the membrane (this takes about 200 ps). The bacteriochlorophyll radical cation P^+ thus formed is reduced by electrons localized on hemes of cytochrome which forms a strong complex with the RC globule in bacteria *Rhodopseudomonas viridis*. As a result, a trans-membrane electron transfer over a distance longer than 60 Å occurs with a quantum yield close to a unity; it is accompanied by an increase in the electron potential which is then converted to the chemical energy.

Yet another example of long-range electron transfer in biological systems is provided by electron transfer in the respiratory chains of mitochondria and some bacteria. At present, it is established that in mitochondria, an electron is successively transferred along the system of metal-containing and organic donor-acceptor sites localized in the large protein complexes **I—III** to reach the final complex

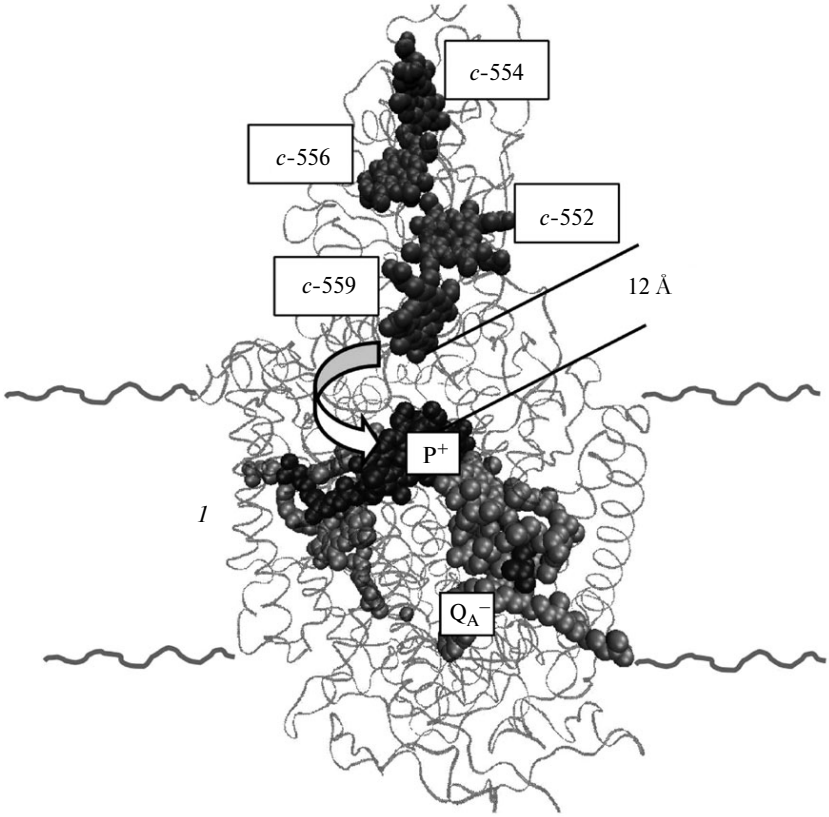

Fig. 1. Structure of a protein complex of a reaction center from photosynthetic bacteria *Rhodopseudomonas viridis* with cytochrome; *1* — membrane. For details, see text.

IV (cytochrome *c* oxidase,[47] see Fig. 2). As a result, transmembrane proton transfer coupled with electron transfer occurs in these membrane proteins. The resulting electrochemical potential gradient on the mitochondrial membrane initiates ATP synthase which synthesizes ATP, a universal biological energy carrier. So far, the structure of complex **IV** is established and the mutual arrangement of the iron-sulfur complexes in complex **I** (NADH—quinone oxidoreductase) is clarified. It was shown that, similarly to processes in the RC of photosynthetic bacteria, activity of the mitochondrial respiratory chain is due to successive electron transfer between the iron-containing centers over distances of 10—15 Å; finally, electrons can travel a distance of about 90 Å by directed movement only within complex **I**.

Analogous electron transfer processes were discovered in studies of the activity of a protein complex — nitrogenase — and some other enzymes.

Thus, main qualitative features of ETR in proteins, including successive one-electron transfer between centers of localization over distances of the order of 5—20 Å and dependence of the transfer rate on the molecular dynamics of the protein were formulated in the beginning of 1990s. Considerable experimental material was obtained and theoretical models for its analysis were developed. However, issues of quantitative description of these reactions and interrelations between the kinetics of electron transfer and the protein structure and dynamic parameters, as well as temperature of the medium remained unsolved.

In this review we briefly outline the simplest models proposed to describe ETR in proteins in the 1990s and different variants of improvements to these models recently proposed by the present authors to describe ETR in RC from photosynthetic bacteria taking into account their molecular dynamics in a wide temperature range.

Electron transfer in metal-containing proteins

Analysis of ETR in the protein structures within the framework of the nonadiabatic approximation. Numerous studies of ETR between donor and acceptor centers in the condensed phase were carried out in the 1970—1980s. The reactions investigated included those between donors and acceptors linked by various organic bridges of different length and nature of the chemical bond; this provided different degree of conjugation of the electron shells of the electron donor and acceptor.[48,49] Most reactions were analyzed within the framework of the nonadiabatic approximation in the theory of outer-sphere electron transfer using the concept of electron tunneling through the matrix

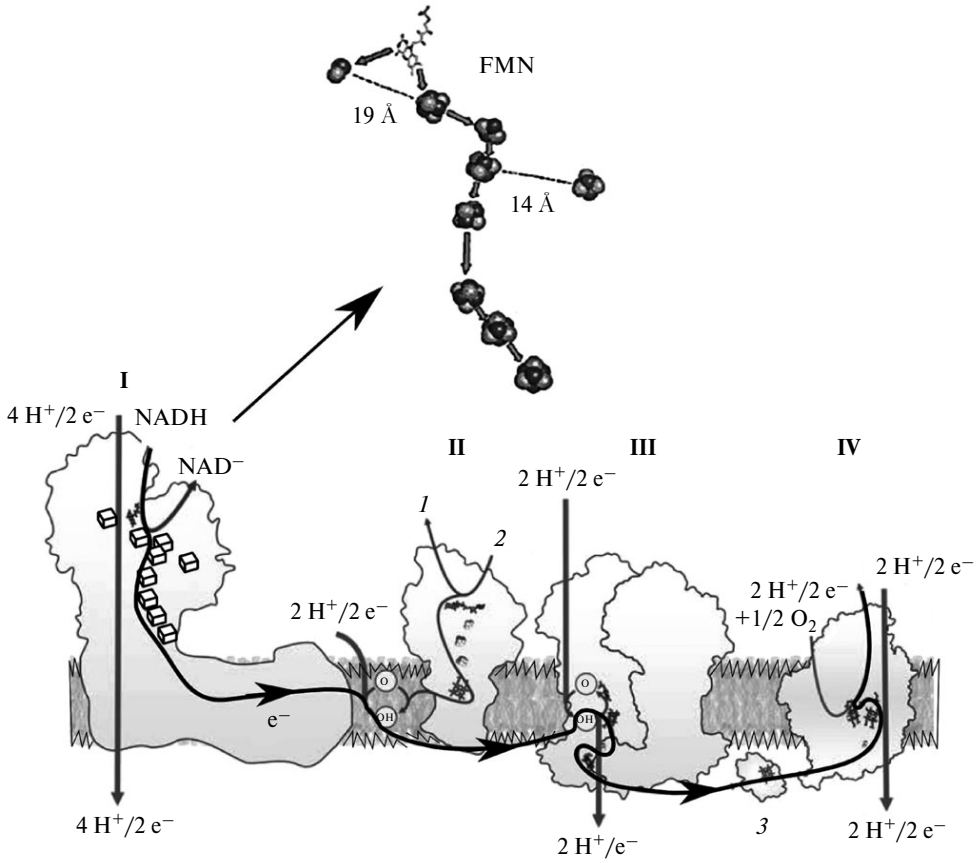

Fig. 2. Mitochondrial respiratory chain: fumarate (*1*), succinate (*2*), and cytochrome *c* (*3*). For details, see text.

or a molecular chain that links the donor and acceptor centers.[50,51] It should be noted that one of the first experiments which gave a convincing proof of the possibility of electron tunneling and a strong impetus to research in this field was a study of ETR in photosynthetic preparations using a pulsed laser.[52] It was found that electron transfer, which slows down as the temperature decreases from ambient temperature to 100 K, becomes temperature-independent on further cooling and can occur at ultralow temperatures down to liquid-helium temperatures.

According to a theory,[50,51] the rate constant for electron transfer k_{et}^{NA} analyzed within the framework of the nonadiabatic approximation assuming fast matrix reorganization is given by

$$k_{et}^{NA} = k_0^{NA}\exp[-(\Delta G + \lambda)^2/(4\lambda k_B T)], \quad (1)$$

where

$$k_0^{NA} = \frac{2\pi V_{ab}^2(R)}{\hbar\sqrt{4\pi\lambda k_B T}}, \quad (2)$$

$$V_{ab}(R) = V_0 \exp\left(-\frac{R}{\hbar}\sqrt{2mH}\right). \quad (3)$$

Here k_0^{NA} is the pre-exponent, V_{ab} is the overlap integral characterizing the quantum effect of the overlap of the donor and acceptor wave functions, ΔG is the Gibbs free energy of the reaction, λ is the nucleus reorganization energy, h is the Planck constant, k_B is the Boltzmann constant, H is the barrier height, and R is tunneling path length. From expressions (1)—(3) it follows that k_{et}^{NA} exponentially depends on the tunneling path length R, being independent of the nucleus reorganization rate $\nu = 1/\tau$, where τ is the dielectric relaxation time. The criterion for applicability of the nonadiabatic approximation is provided by the value of the adiabaticity parameter $\eta = 4\pi V_{ab}^2\tau/(h\lambda)$, *viz.*, for a nonadiabatic reaction one has $\eta << 1$ (weak electron interaction and fast relaxation of the medium).

Taking into account the exponential dependence of the parameter $V_{ab}(R)$ characterizing the overlap between the electron shells of the donor and acceptor centers on the distance between them, expression (1) can be written as

$$k_{et}^{NA} = k_0\exp(-\alpha R). \quad (4)$$

The parameter α characterizes the degree of delocalization of the electron shells of the donor and acceptor centers in the matrix to be analyzed, including delocalization due to superexchange interactions, and can serve as a measure of the matrix conductivity. From relationships

(1)—(4) it follows that k_{et}^{NA} exponentially depends on the distance R, quadratically depends on λ, and reaches a maximum at $-\Delta G = \lambda$.

The first quantitative analysis summarizing the data on the rate of electron transfer in various protein structures (including RC, heme-containing proteins hemoglobin, myoglobin, cytochrome *c*, and a copper-containing protein azurin) within the framework of the theory of outer-sphere electron transfer was reported in Refs 53—55. Analysis of experimental data revealed a reasonable agreement between a large array of data on the reaction rates and theoretical predictions provided that the "distance" is defined as the separation between the electron transfer sites (or between the frontier π-orbitals of porphyrin structures of the metal-containing sites). Using expression (4), a linear dependence of the rate constant for electron transfer k_{et}^{NA} on the distance R between the transfer centers in various proteins[53—57] was obtained in the semilogarithmic coordinates (Fig. 3). This made it possible to determine the parameter $\alpha = 1.4$ Å^{-1} for these proteins; α quantitatively characterizes the ability of the protein matrix to assist tunneling of an electron between centers through superexchange interaction of the donor and acceptor orbitals. The best correlation was obtained for the experimental data on electron transfer in RC.

The fact that a large number of points lies below the straight line suggests nonoptimum reaction conditions, *e.g.*, if the condition $-\Delta G = \lambda$ is not met. Indeed, studies of electron transfer over specified distances in particular proteins (ΔG values were changed by varying the redox potential of the donor or acceptor) revealed parabolic dependences of k_{et}^{NA} on ΔG suitable for the determination of the

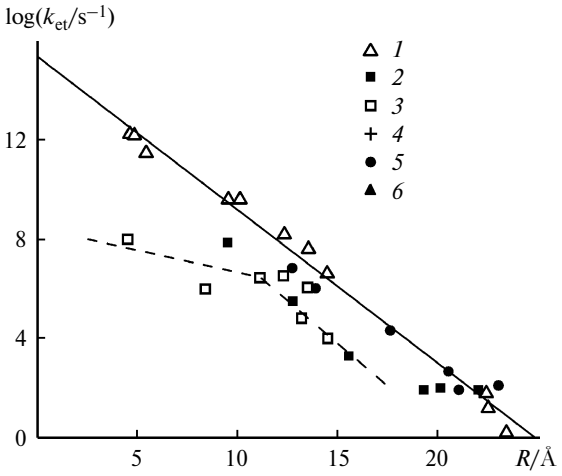

Fig. 3. Rate constant for electron transfer k_{et} as a function of distance R between the closest points of conjugated electron shells of donor and acceptor centers localized in proteins: reaction centers of photosynthetic bacteria[55] (*1*), myoglobin[6,16] (*2*), cytochrome *c*[14,15] (*3*), hemoglobin[22] (*4*), azurin[8] (*5*), and protein complexes cytochrome *c*—cytochrome b_5 and cytochrome *c*—cytochrome *c* peroxidase[12,21] (according to Refs 55 and 56) (*6*).

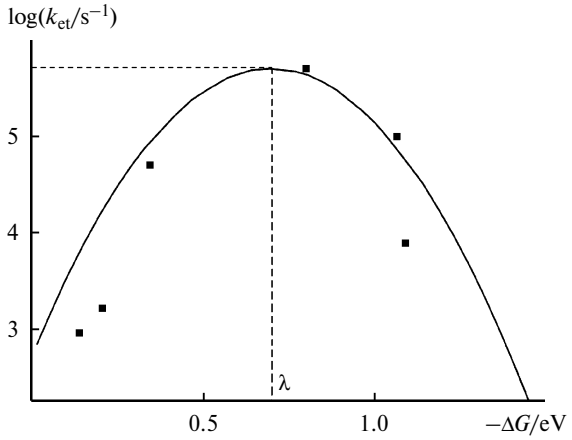

Fig. 4. The rate constant k_{et} as a function of ΔG for electron transfer in the structure of the protein complex cytochrome *c*—cytochrome b_5.[12]

corresponding λ values[6,12,55] (Fig. 4). The maximum k_{et}^{NA} values determined taking into account these parabolic dependences better agree with the overall linear dependence of $\log k_{et}^{NA}$ on R.

Based on analysis of experimental data (see Figs 3 and 4), one can conclude that electron transfer can occur efficiently in different types of proteins over distances 5—25 Å on the time scale from 10^{-12} to 10^{-1} s. A common exponential dependence of k_{et}^{NA} on R and parabolic dependences of k_{et}^{NA} on ΔG for a wide range of reaction rate constants and various proteins suggest that the nonadiabatic model of electron transfer can to a first approximation be applied to analysis of electron transfer in proteins, even if particular molecular structures of the proteins are ignored and they are treated as isotropic matrices characterized by the parameter $\alpha = 1.4$ Å^{-1}. However, Fig. 3 shows that a number of experimental data appreciably deviate from the overall linear dependence. In particular, this is valid for cytochrome *c*, especially for its short-range electron transfer reactions (4—10 Å).[14,15]

To more accurately account for specific features of a particular protein structure within the framework of the nonadiabatic model, reactions of electron transfer in protein globule along a specified optimum direction were analyzed.[10,13,58] Allowance was made for the structural features of proteins consisting of polypeptide chains in which all amino acids have the same structure along the chain and only differ in the side amino acid residues. Within the framework of the superexchange approximation, it was assumed that one can select an optimum, most effective trajectory of electron transfer in the protein structure. One portion of the trajectory corresponds to electron transfer along the polypeptide chain, whereas the other portion corresponds to an electron jump between the polypeptide chains through hydrogen bonds or simply through space between atoms (through vacuum). For any portion of the electron transfer trajectory one can introduce some coeffi-

cients α_1, α_2, and α_3, respectively, which should be universal for different proteins. Taking into account the exponential dependence of k_{et}^{NA} on the electron transfer path length R, within the framework of this approach k_{et}^{NA} can be represented by the product of three exponents with the corresponding values α_i by the effective distances R_i for all types of bonds (see expression (3)). Using this approach, experimental data for azurin[19] and cytochrome *c* (see Ref. 13) were described correctly; somewhat poorer results were obtained for myoglobin.[10] However, a comparison of the available experimental data on electron transfer in the structures of all three proteins revealed no internally consistent dependences. An attempt to improve the model by considering the possibility of simultaneous electron transfer along a number of trajectories rather than a single optimum trajectory was undertaken.[14] However, this approach also failed to describe the totality of experimental results with sufficient accuracy. A more detailed analysis of these dependences was reported in two reviews.[56,57]

Analysis of ETR in proteins within the framework of adiabatic approximation. The observed deviations of experimental data from the overall linear dependence of $\log k_{et}$ on the tunneling path length R can be explained within the framework of adiabatic approximation to the theory of outer-sphere electron transfer.

As mentioned above, the use of the nonadiabatic approximation depends on the ratio between V_{ab} and ν, which can vary over a wide range for proteins. The estimates obtained for electron transfer over distances of 12—15 Å in RC and other metal-containing proteins are as follows: $V_{ab} = 10^{-1}$—10^{-2} cm^{-1} (10^{-5}—10^{-7} eV).[13,14,16] Assuming $\lambda = 1$ eV for these reactions, the nonadiabaticity condition $\eta << 1$ will be met at $\nu >> 10^7$ s^{-1}. Studies of some proteins including cytochrome *c* and hemoglobin by various physical methods showed that ETR in the matrix are accompanied by dynamic processes with frequencies up to $\nu = 10^6$—10^3 s^{-1}.[4,29—31,33—34,36—38,40—42] For these reactions, the nonadiabaticity condition is not met and one should use[59,60] the adiabatic approximation, according to which

$$k_{et}^{AD} = \nu A \exp[-E_a/(k_B T)], \quad (5)$$

where $E_a = (\Delta G + \lambda)^2/(4\lambda)$, $A = (\varepsilon_s/\varepsilon_\infty)[\lambda/(16\pi k_B T)]^{0.5}$, ε_s and ε_∞ are the dielectric constants obtained from static measurements and in the high-frequency limit, respectively. From expression (5) it follows that in this approximation the k_{et}^{AD} value is determined by the molecular dynamics of the medium specified by the parameter ν; also, k_{et}^{AD} is independent of the overlap integral V_{ab} and, consequently, of the electron transfer path length R.

If the nonadiabaticity condition is not rigorously met, it was proposed[61] to use the following relation

$$k_{et} = \frac{k_0^{NA}}{1 + k_0^{NA}\tau/A} \exp\left(-\frac{E_a}{k_B T}\right), \quad (6)$$

which gives the nonadiabatic limit at $k_0^{NA}\tau/A << 1$ and the adiabatic limit at $k_0^{NA}\tau/A >> 1$.

Differences in the functional dependence of k_{et} on R and ν, obtained in the nonadiabatic and adiabatic approximations are very important for analysis of ETR in proteins because R and ν are determined by the spatial and dynamic organization of macromolecules and can vary from one protein to another. Taking account of this fact can play a decisive role for correct quantitative analysis of experimental data. In particular, substituting the k_{et}^{NA} value from expression (4) into Eq. (6) gives a combined relation between k_{et} and R. No dependence was found for short distances and an exponential dependence was detected for long distances, as was observed for cytochrome *c* (see Fig. 3). From Fig. 3 it follows that the nonadiabaticity condition for cytochrome *c* is no longer valid at characteristic times of the order of 10^{-6}—10^{-7} s. The occurrence of relaxation rearrangements of the protein globule in the vicinity of the heme on pulsed reduction of cytochrome *c* or other heme proteins on the time scale from 10^{-6} to 10^{-3} s even at room temperature was experimentally confirmed by various physical methods.[37,38]

Yet another indication of adiabatic mechanism of electron transfer in proteins is provided by the existence of relevant temperature dependences[6,9,20,23,25,26] (Fig. 5). The temperature or solvent viscosity dependences of electron transfer rates in RC from photosynthetic bacteria, in heme-containing proteins, and in azurin could not be explained only within the framework of the nonadiabatic approximation, without considering the molecular dynamics of the matrix. For instance, the rate of photostimulated electron transfer between a ruthenium complex and Zn-substituted porphyrin in cytochrome *c* (see Ref. 9) or in myoglobin[6] increases in a wide temperature range (120—260 K). However, for the complex cytochrome *c*—cytochrome *c* peroxidase a similar transfer is observed in a narrow tem-

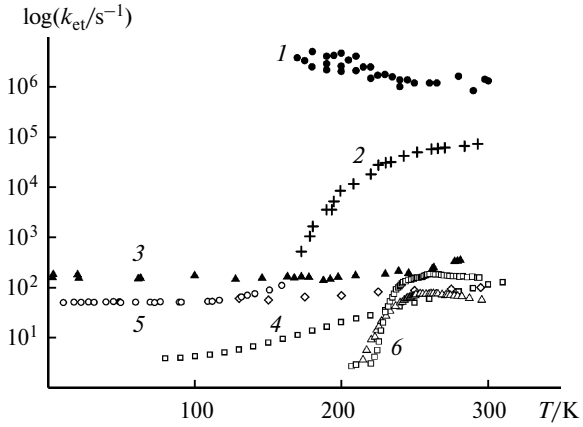

Fig. 5. Temperature dependences of k_{et} for electron transfer reactions in metal-containing proteins: azurin[20] (*1*), myoglobin[6] (*2*), hemoglobin[25,26] (*3*, *4*), cytochrome *c* (*5*)[9], and complex cytochrome *c*—cytochrome *c* peroxidase[23] (*6*).

perature range (220—250 K)[23] while the rate of electron transfer in azurin[20] and in hemoglobin[25,26] remains unchanged in a wide temperature range from ambient to helium temperatures. These differences can be explained by the fact that the major contribution to the increase in the reaction rate comes from different types of motion. These range from fast vibrational degrees of freedom in cytochrome *c* and myoglobin to slow diffusion motions at temperatures above the glass transition temperature in the protein complex cytochrome *c*—cytochrome *c* peroxidase.

In myoglobin, the rate of electron transfer from triplet excited eosin to the protein heme increases in the temperature interval 170—178 K; the molecular dynamics on the protein surface whose characteristic times are comparable with those of electron transfer also manifests itself in this temperature range.[42,57]

The molecular dynamics on the millisecond time scale was analyzed by recording the kinetics of the shift of the phosphorescence spectrum of eosin, characteristic of the dipole orientational reorganization of the matrix. Further studies showed that the temperature corresponding to an increase in the electron transfer rate and to a shift of the phosphorescence spectrum increases with the increase in the solvent viscosity. Thus, an important role of the molecular dynamics in ETR and the need to use the adiabatic approximation to describe these reactions in heme-containing proteins, especially at low temperatures became obvious.

A similar consideration is also valid for ETR in RC. The temperature and solvent composition affect the rates of particular steps of electron transfer in RC of photosynthetic bacteria and the changes in the molecular dynamics of the protein matrix detected by various physical methods under these conditions.[27,28,31—34,62,63] Significant changes in the parameters characterizing the kinetics of electron transfer between the proximal heme *c*-559 of the cytochrome subunit and the bacteriochlorophyll dimer radical cation P^+ in *Rps. viridis* in the temperature range from ambient to helium temperatures, as well as in other steps of ETR in RC (Fig. 6) were observed.[64—68] The rate of electron transfer in RC changes as the solvent viscosity or composition changes.[34,62,63] These effects were usually explained by the modification of the protein structure caused by changes in temperature, solvent polarity, or the system of hydrogen bonds. The transfer path length and the thermodynamics of the reaction can also be subjected to changes; according to expressions (1)—(4), this should lead to a change in the electron transfer rate. However, in reality the protein structure and the redox potential of the electron transfer centers can remain uncnahged and considerable changes in the electron transfer rate following from relations (5) and (6) can probably be caused by the changes in the molecular dynamics of the protein globule.

Although on the qualitative level the role of the molecular dynamics of chromophores and RC in ETR was revealed by various physical methods,[27,28,31—33,61—63] studies on quantitative description of the reaction rate and its relation to the real physical parameters of the protein structure and the medium have long been scarce and some relationships were established only within the framework of the nonadiabatic approximation without using parameters characterizing the protein dynamics. For instance, the dielectric behavior of RC in ETR was considered[69] within the framework of the nonadiabatic model using a time-dependent dielectric constant ε_τ and, therefore, time-dependent reorganization energy λ. In other series of studies the temperature dependence of the reaction rate and the nonexponential character of the kinetic curves were explained within the framework of the nonadiabatic approach by the effect of a distribution over ΔG and its changes with temperature.[70—72]

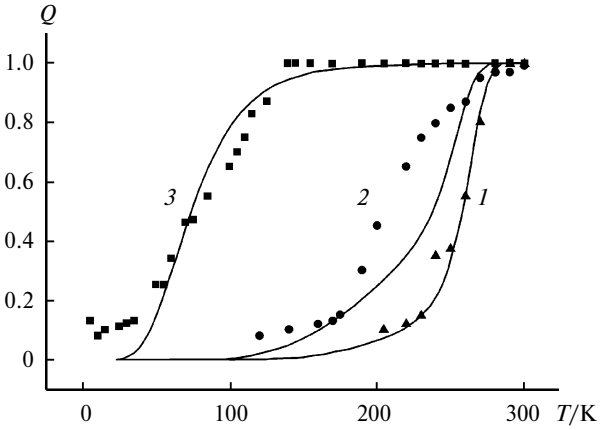

Fig. 6. Temperature dependences of the effective parameter *Q* characterizing the efficiency of electron transfer in RC from *Rps. viridis* for different reduction states of cytochrome hemes: only heme *c*-559 is reduced (*1*), hemes *c*-559 and *c*-556 are reduced (*2*), and hemes *c*-559, *c*-556, and *c*-551 are reduced (according to Ref. 66) (*3*). Solid lines: results of simulation within the framework of empirical two-mode model.[57]

The kinetics of electron transfer in RC from *Rps. viridis* was analyzed[65—68] within the framework of the multiexponential expansion or using the effective empirical parameter *Q* corresponding to the amplitude of the fast component of the kinetic curve at $t = 10$ μs after excitation. Based on the available experimental data,[65—68] the temperature dependences of the effective parameters of electron transfer in the RC of photosynthetic bacteria *Rps. viridis* from the reduced heme of cytochrome *c*-559 to the bacteriochlorophyll dimer radical cation P^+ were explained[73] by joint influence of two factors. These are the molecular dynamics of the protein globule and the change in the electron energy level on the heme *c*-559 due to electrostatic interaction of this electron with the extra electrons during the reduction of the hemes *c*-556 and *c*-552. However, although the molecular dynamics of the protein during ETR plays an important role, the observed rate

constants were analyzed[73] within the framework of the nonadiabatic approximation, according to which the rate of the relaxation process in the matrix should not affect the kinetics of electron transfer. The last theory can´t be reconciled with the dependence of the initial rate of electron transfer in these RC on temperature for all degrees of reduction of the cytochrome.[66]

Analysis of the nonexponential kinetic curves at different temperatures and cytochrome reduction states suggests that the characteristic times of electron transfer in this protein complex can differ by more than four orders of magnitude.[64,68] In the early investigations of these reactions it was assumed that the changes in the transfer rate can simply be due to the changes in the distance between the donor and acceptor centers caused by changes in temperature. However, an analysis within the framework of the nonadiabatic approximation using expression (4) showed that such large differences in the electron transfer rate can not be explained only by the conformational changes of the protein or by the temperature-dependent variations of the parameters ΔG and λ.

In the subsequent Sections of this review the emphasis will be placed on the analysis of experimental data describing electron transfer in RC of photosynthetic bacteria from the reduced proximal heme *c*-559 of cytochrome to the bacteriochlorophyll dimer radical cation P^+ in RC from two types of bacteria, *Rps. viridis* and *Rps. sulfoviridis,* taking into account the molecular dynamics of the protein globules.[57,74–79]

Electron transfer reactions in reaction centers of photosynthetic bacteria

Specific features of ETR in RC. Studies of ETR in RC is of particular interest for some reasons.

Photoexcitation of the primary donor P (bacteriochlorophyll dimer) with a laser pulse causes an electron to be transferred to the primary acceptor, quinone Q_A.[80] This can be followed by reduction of P^+ through direct electron transfer from the reduced proximal heme *c*-559 or through back electron transfer from Q_A^-. The cytochrome structure contains the hemes *c*-559, *c*-552, *c*-556, and *c*-554 with the reduction potentials of +380, +20, +310, and −60 mV, respectively.[81]

The reactions of electron transfer from the reduced proximal heme *c*-559 of cytochrome to the bacteriochlorophyll dimer radical cation P^+ in RC from *Rps. viridis* were experimentally investigated in a wide temperature range at different degrees of reduction of the cytochrome hemes *c*-559, *c*-556, and *c*-552.[65–68]

It was found that the kinetic curves of changes in P^+ absorption, which describe ETR in the RC of *Rps. viridis*, show an essentially nonexponential character in a wide temperature range from 295 to 40 K and that the parameter *Q* describing their changes with temperature also depends on the reduction state of other cytochrome hemes (see Fig. 6). As can be seen from Figure 6, the reduction of the hemes *c*-556 and *c*-552 causes these temperature dependences to shift toward lower temperatures.

The structure of the protein complex on the pathway of electron transfer between the heme *c*-559 and bacteriochlorophyll dimer P^+ in these RC was the subject of a high-precision X-ray study (Fig. 7).[46] In this case, the transfer path length is fixed (12.3 Å between the outermost points of the π-electron orbitals of *c*-559 and P^+).

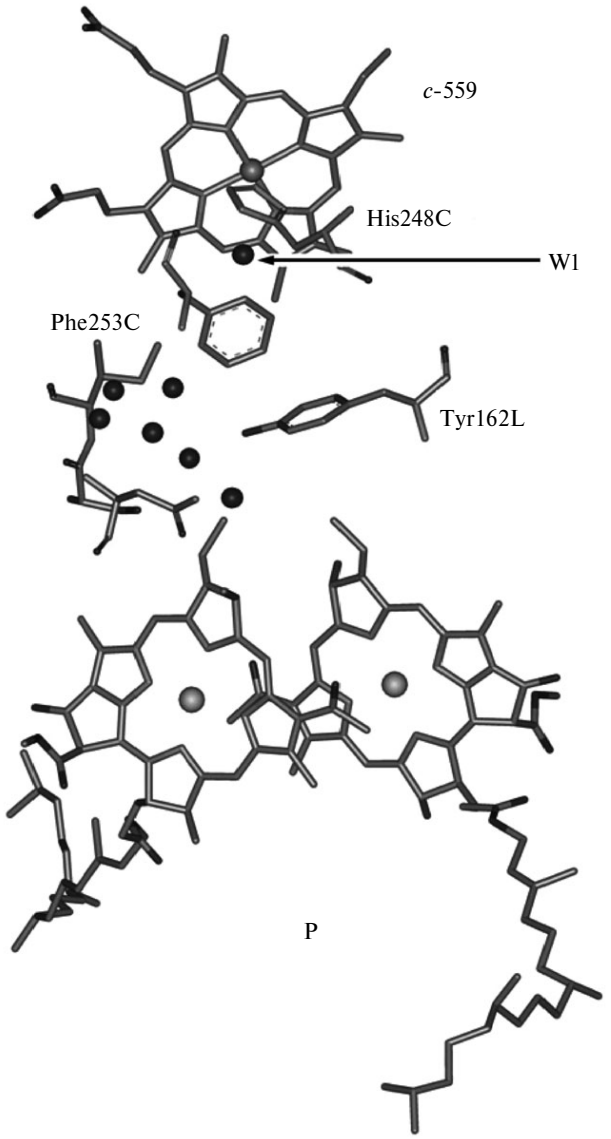

Fig. 7. Structural fragment of a protein complex of RC from *Rps. viridis*: an electron is transferred from the heme *c*-559 to the bacteriochlorophyll dimer P^+. Shown are water molecules in the protein structure (PDB code, 1PRC) between the heme *c*-559 and P. Water molecule W1 (HOH38) forms hydrogen bonds with histidine ligand of the heme *c*-559 and with the neighboring phenylalanine residue; this may have strong effect on electron transfer.[46]

In the subunit L of the reaction center, the pathway of electron transfer between *c*-559 and P^+ passes through a side tyrosine residue L162Y. Clearly, replacement of this residue by some other amino acid can lead to changes in the number of the key parameters, such as the matrix element V_{ab}, reorganization energy λ, and relaxation frequency ν; eventually, this will cause changes in the rate of electron transfer.

The amino acid Tyr-162 was replaced by six other amino acids and the kinetics of ETR in the mutant RC was studied.[67,68] It was found that replacement of the amino acid does significantly influence the kinetics of electron transfer; however, the first publications of these experimental results included only a primary qualitative analysis of the kinetic dependences.

Then, a series of experimental studies on the kinetics of electron transfer in RC from *Rps. sulfoviridis* was carried out. It is known[82] that the spectroscopic and biochemical characteristics (absorption spectra and reduction potentials of bacteriochlorophyll dimer P and cytochrome hemes) of these RC are similar to those of the protein complex from *Rps. viridis*. Although the spatial structure of the RC from *Rps. sulfoviridis* was not studied as yet, in the analysis we assume that this RC is structurally similar to the protein complex from *Rps. viridis*.

Studies of all types of RC revealed that the reaction in question obeys common kinetic regularities discovered earlier[65—68] for *Rps. viridis*. The kinetic curves of changes in absorption of P^+, which describe ETR in RC, are essentially nonexponential in a wide temperature range from 295 K down to helium temperatures, being dependent on the reduction state of the cytochrome hemes (Figs 8 and 9). From Figures 8 and 9 one can see that in the first reduction state of cytochrome (only the heme *c*-559 is reduced) a noticeable change in the kinetics of ETR occurs in the temperature range from 295 to 220 K, whereas further decrease in temperature leaves the kinetic curves almost unchanged. In the second reduction state of cytochrome (the hemes *c*-559 and *c*-556 are reduced), the temperature range of changes extends down to 170 K. In the third reduction state (three hemes, *viz.*, the hemes *c*-559, *c*-556 and *c*-552 are reduced), decreasing rates of electron transfer are observed down to 40 K (see Fig. 9).

After excitation of the primary donor P, an electron is transferred to the primary acceptor Q_A.[80] This can be followed by the reduction of P^+ due to direct electron transfer from the reduced proximal heme *c*-559^- or due to the reverse electron transfer from Q_A^- according to the scheme

$$c\text{-}559^- \xrightarrow{k_{et}} P^+ \xleftarrow{k_r} Q_A^-.$$

If the direct reaction proceeds on the microsecond time scale, the reverse reaction $Q_A^- \rightarrow P^+$ is much slower, *viz.*, $k_r = (1—4) \cdot 10^2\ s^{-1}$ in the temperature range 100—295 K.[83]

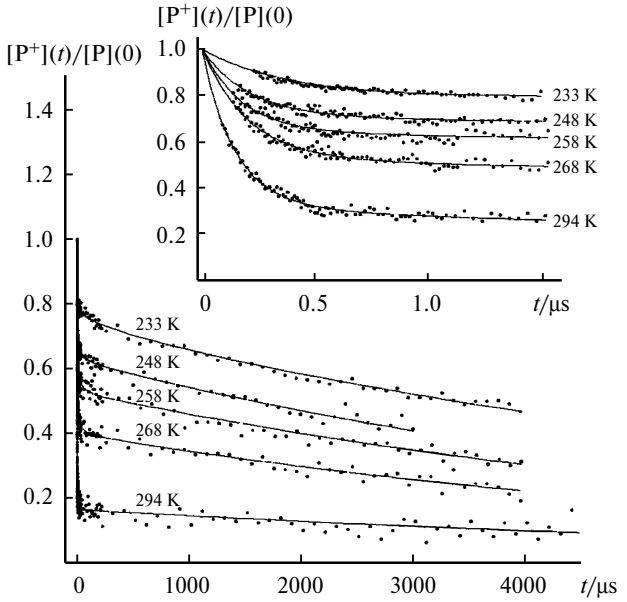

Fig. 8. Kinetic curves of reduction of radical cation P^+ in RC from *Rps. sulfoviridis* at different temperatures. Cytochrome in the first reduction state (heme *c*-559 is reduced, $E_{1/2} = +360$ mV). Points denote experimental data; solid lines represent the results of computer simulation using the combined two-mode model.[74,75] Inset: initial portions of the kinetic curves.

Preliminary analysis of the time dependence of the function $F(t) = [P^+](t)/[P^+](0)$ describing the evolution of P^+ after excitation shows that on a long time scale from 0.1 to 4500 μs at different temperatures all experimental data can be represented by the sum of two strongly different curves (see Fig. 8). The initial portion of the kinetic curves in the interval 0.1—40 μs is fast, temperature-dependent, and nonexponential, whereas at 40 μs < t < 4500 μs, the curves decay slowly and show a monoexponential behavior with a rate constant in the range $(1—4) \cdot 10^2\ s^{-1}$, being almost independent of temperature. Since the characteristic rates of the initial portions of the kinetic curves ($k_{et} = 10^7—10^4\ s^{-1}$) are much higher than the rate of the reverse reaction $P^+ \leftarrow Q_A^-$, it seems reasonable to attribute the fast nonexponential portion of the curve to the reaction *c*-$559^- \rightarrow P^+$ and the slow exponential portion to the recombination $P^+ \leftarrow Q_A^-$.

The results of successive analysis[57,74—79] of all kinetic curves obtained for the RC listed above and for their mutant modifications using different models taking into account the molecular dynamics of proteins will be briefly outlined below. For more accurate description of the kinetic curves of ETR in various RC in a wide temperature range we used the Rips—Jortner model,[61] the Sumi—Marcus model,[84] as well as new modified forms of these models.

Analysis of the initial portions of the kinetic curves of electron transfer within the framework of the Rips—Jortner approximation. To analyze the ETR which can be controlled by the dynamics of the matrix, it was proposed[61] to

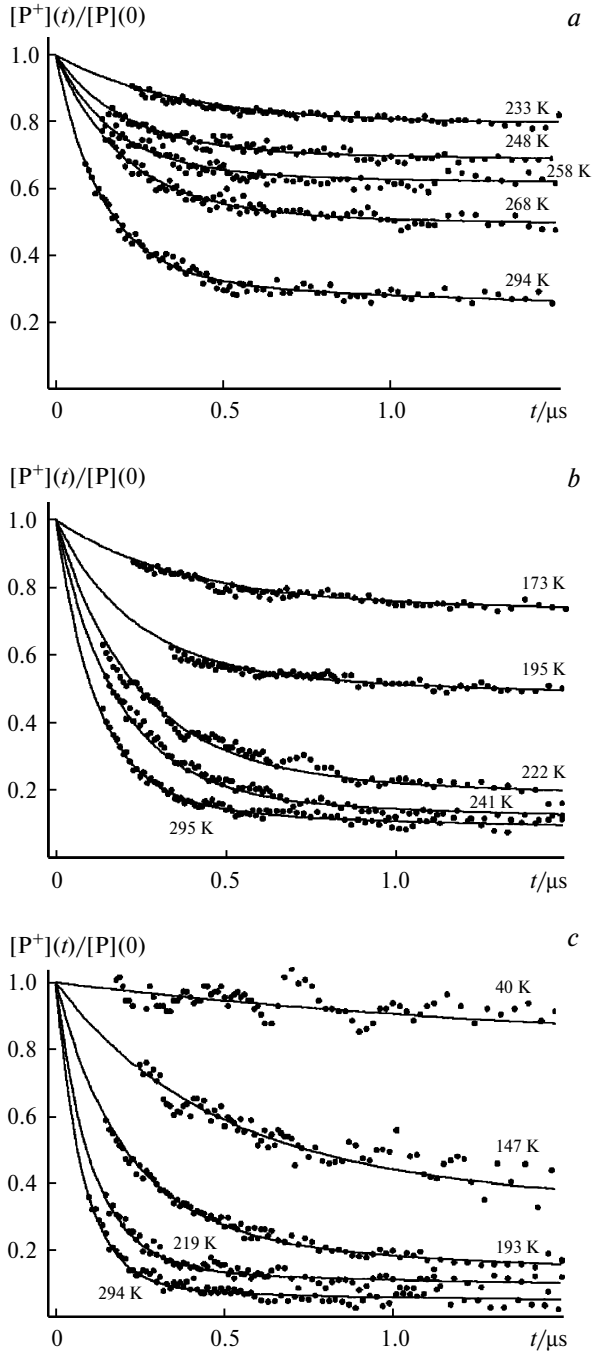

Fig. 9. Kinetic curves of reduction of radical cation P^+ in RC from *Rps. sulfoviridis* at different temperatures and reduction states of cytochrome on the time scale of 1.5 μs: *a* — heme *c*-559 is reduced ($E_{1/2}$ = +360 mV); *b* — hemes *c*-559 and *c*-556 are reduced ($E_{1/2}$ = +250 mV); *c* — hemes *c*-559, *c*-556, and *c*-552 ($E_{1/2}$ = −20 mV). Points denote experimental data; solid lines represent the results of computer simulation using the combined two-mode model.[74,75]

use expression (6). Let us assume that the characteristic times of relaxation processes in the matrix are determined by the Cole—Davidson distribution

$$g(\tau) = \frac{\sin(\pi\beta)}{\pi\tau}\left(\frac{\tau}{\tau_0 - \tau}\right)^{\beta}, \quad 0 < \tau < \tau_0, \qquad (7)$$

$$g(\tau) = 0, \qquad \tau > \tau_0$$

where β ($0 \le \beta \le 1$) is Cole—Davidson distribution parameter and τ_0 is the characteristic relaxation time corresponding to the maximum observed dielectric relaxation time τ.[82] Substituting the distribution (7) into relation (6) and integrating over time from 0 to τ_0 yields analytical expressions for the average rate constant at the initial time

$$k_{et} = \frac{1}{h}\left(\frac{\varepsilon_0}{\varepsilon_\infty}\frac{h}{4}\right)^{\beta}\left(\frac{\pi}{4\lambda k_B T}\right)^{0.5} \cdot$$
$$\cdot V_{ab}^{2(1-\beta)}\left(\frac{1}{\tau_0}\right)^{\beta}\exp\left[-\frac{(\Delta G + \lambda)^2}{4\lambda k_B T}\right]. \qquad (8)$$

At β = 0, this expression is transformed to relationship (1) which describes the nonadiabatic approximation. At β = 1, one gets expression (4) which describes the adiabatic approximation.

The Rips—Jortner model was used[74,76] to analyze the temperature dependences of the initial rate constants k_{et} for ETR between the heme *c*-559 and the bacteriochlorophyll dimer P^+ in the RC from *Rps. viridis*. The k_{et} values were determined from the slope of the initial portion of the kinetic curves and normalized to the amplitude A_1. The k_{et} values thus obtained at different temperatures and degrees of reduction of the hemes *c*-559, *c*-556, and *c*-552 are shown in Fig. 10.

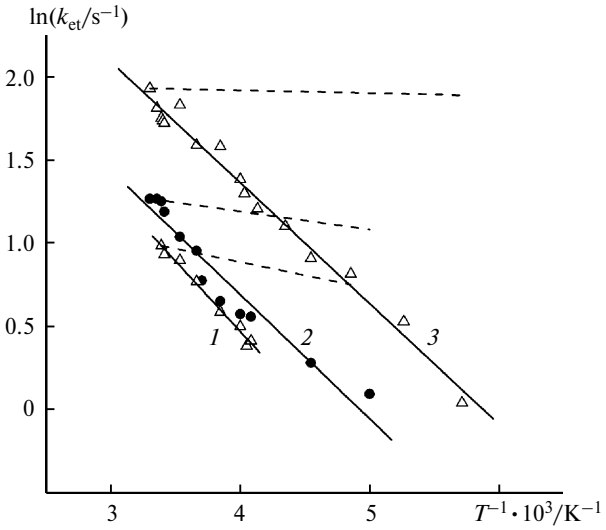

Fig. 10. Arrhenius plots of the average initial rate constants k_{et} for three different reduction states of cytochrome: *1* — heme *c*-559 is reduced ($E_{1/2}$ = +360 mV); *2* — hemes *c*-559 and *c*-556 are reduced ($E_{1/2}$ = +250 mV); *3* — hemes *c*-559, *c*-556, and *c*-552 are reduced ($E_{1/2}$ = −20 mV). Dashed lines represent the Arrhenius plots of k_{et} for different reduction states of cytochrome calculated from expression (1) using ΔG_1 = 0.14 eV, ΔG_2 = 0.16 eV, ΔG_3 = 0.22 eV and λ = 0.26 eV.[76]

Analysis of experimental data was carried out in two steps. Initially, it was suggested that the data obtained at room temperature (the case for high protein mobility) can be analyzed in the nonadiabatic approximation. Using this approach, it was shown[73] that general regularities of changes in the effective parameters of ETR can be described on the assumption that these temperature-induced changes are due to the joint influence of the molecular dynamics of the protein globule and the change in the energy level of the electron attached to the heme *c*-559 owing to electrostatic interaction of this electron with the extra electrons in the reduction of the hemes *c*-556 and *c*-552. In addition, it was assumed that in the second (the heme *c*-556 is also reduced) or third steps of the reduction (the hemes *c*-556 and *c*-552 are reduced) one has $\Delta G_i = \Delta G_1 + \delta_i$ and $H_i = H_1 - \delta_i$. In these equations, ΔG_1 and H_1 are the free energy of reaction and the tunneling barrier height for the first degree of protein reduction (only the nearest, with respect to P^+, heme *c*-559 is reduced), δ_i is the energy of electrostatic interaction between the electron attached to the heme *c*-559 and electrons attached to the hemes *c*-556 ($i = 2$) and *c*-552 ($i = 3$). Using this approach and assuming $-\Delta G_3 = \lambda$, the following values were reported: $\Delta G_1 = -0.14$ eV, $\Delta G_2 = -0.18$ eV, $\Delta G_3 = -0.29$ eV, and $\lambda = 0.29$ eV.

The ratio of the rate constants for the reaction in different reduction states of the cytochrome hemes derived from expressions (1)—(3) within the framework of the nonadiabatic approximation has the form

$$\frac{k_1}{k_i} = \exp\left[\frac{2R}{h}\sqrt{2m}\left(\sqrt{H} - \sqrt{H - \delta_i}\right) + \frac{2\delta_i(\Delta G_1 + \lambda) + \delta_i^2}{4\lambda k_B T}\right], \quad (9)$$

where $i = 2, 3$.

Using the values $\Delta G_1 = -0.14$ eV, $H = 1.9$ eV, and $R = 12.3$ Å,[73] from relationship (2) one can determine λ at specified parameters δ_i. When choosing the δ_2 and δ_3 values, it was assumed that the energy of electrostatic interaction between the hemes *c*-559 and *c*-552 (δ_2) is 0.01 eV and the energy of electrostatic interaction between the hemes *c*-559 and *c*-556 ($\delta_3 - \delta_2$) is 0.06 eV.[86] Expression (9) gives the best agreement with the experimental data at $\lambda = 0.26$ eV, when $\delta_2 = 0.02$ eV, and $\delta_3 = 0.06$ eV.

Therefore, within the framework of the nonadiabatic approximation for the room-temperature reactions one gets $\Delta G_1 = -0.14$ eV, $\Delta G_2 = -0.16$ eV, $\Delta G_3 = -0.22$ eV, and $\lambda = 0.26$ eV. According to expression (1), the activation energies of the corresponding processes are equal to $E_a^1 = 0.014$ eV, $E_a^2 = 0.009$ eV, and $E_a^3 = 0.0014$ eV. As can be seen from Fig. 10, the activation energy values thus calculated disagree with the experimental dependences (dashed lines). The temperature dependences of k_{et} are linear in the Arrhenius coordinates with the activation energies $E_a^1 = 0.073 \pm 0.015$ eV, $E_a^2 = 0.064 \pm 0.006$ eV, $E_a^3 = 0.062 \pm 0.005$ eV for the first, second, and third reduction states of cytochrome, respectively.

To overcome this contradiction, one can bear in mind that, according to expression (8), the activation energy corresponding to the average initial rate constant k_{et} can be represented by the sum

$$\tilde{E}_a^i = E_r\beta + E_a^i, \quad (10)$$

where $E_r\beta$ is part of the total activation energy from the term $\tau_0^{-\beta}$ in expression (8), which characterizes the dynamics of the medium while E_a^i is the activation energy using ΔG_i and λ according to expressions (1) and (8).

Using formula (10) and the E_a^i and E_a^i values listed above, one gets $E_r\beta = 0.052$ eV. As E_r, one can use a value of 0.23 eV, which is readily obtained based on the temperature dependence of the average relaxation time $\tau_{av} = \tau_0\beta$ using the τ_0 and β values obtained[43] by analyzing the diffusion displacements of the Fe atom in the myoglobin heme by Mössbauer spectroscopy within the framework of the Cole—Davidson formalism. This gave $\beta = 0.23$, which is in good agreement with the β values determined in the Mössbauer spectroscopy studies of the dynamics of myoglobin in temperature range 232—245 K.[43]

Substitution of the calculated ΔG_1, ΔG_2, ΔG_3, λ, and β values as well as other parameters into expression (8) and subsequent analysis of experimental data using the k_1/k_i ratios, as was done earlier within the framework of the nonadiabatic approximation, gives good agreement.

The numerical values thus obtained allow one to calculate the characteristic time of the protein relaxation rearrangement from relation (8) assuming that $V_{ab} = 1.6 \cdot 10^{-5}$ eV (see Ref. 82) and $\varepsilon_0/\varepsilon_\infty = 2$, which is usually accepted for internal hydrophobic fragments of protein globules. This approximation gives for RC from *Rps. viridis* a room-temperature value $\tau_0 = 0.17$ μs, which agrees well with the results of measurements of the protein dynamics in RC by Mössbauer spectroscopy.[73]

This analysis shows that the Rips—Jortner approximation allows one to consistently describe the initial portions of the experimental kinetic curves of electron transfer in RC of photosynthetic bacteria taking into account the internal molecular dynamics of the protein complexes. Accordingly, reasonable estimates of all physical parameters of this model can be obtained.

However, this formalism is only valid for the initial portions of the kinetic curves and seems to be inappropriate for the description of the whole kinetic curves. For complete description of experimental data in a wide temperature range we proposed an empirical two-mode model based on the Sumi—Marcus approximation.

Empirical two-mode model. The temperature dependences of the effective parameter Q characterizing the rate of electron transfer in RC at different degrees of reduction of cytochrome *c* (see Fig. 6, Ref. 66) were described using the two-mode model.[84,87]

Within the framework of this model, relation (1) was modified taking into account the assumption of energy

dissipation during electron transfer *via* two (namely, vibrational and diffusional) degrees of freedom simultaneously.[5] Indeed, diffusion in proteins is always accompanied by vibrational (nondiffusion) motions characterized by very short relaxation times; they are not "frozen" at very low temperatures. The free energy surface for this type of reactions is shown in Fig. 11. If the motion along both coordinates (vibrational coordinate q and diffusion coordinate X_1) is fast, the reaction follows an optimum, fastest nonadiabatic trajectory *1* from point B_1 to point C with the minimum activation energy E_a^{min} at the point S_1 corresponding to the transition state of the reaction. However, if the rate of the motion along the diffusion coordinate X_1 decreases as temperature decreases and ETR along the diffusion coordinate becomes formally adiabatic, effective electron transfer still continues owing to the possibility for the reaction to proceed mainly along the vibrational coordinate *via* another transition state with higher activation energy. Since relaxation along the vibrational coordinate is fast and electron transfer along this coordinate is always nonadiabatic (for ETR on the microsecond time scale). In this case the reaction proceeds in a combined adiabatic-nonadiabatic regime along pathway *2* which intersects the line of transition states at the point S_2.

This shift of the transition state can phenomenologically be described by the relations

$$k_{et}(\tau) = \sigma(\tau)\exp[-E_a(\tau)/(k_B T)], \quad (11)$$

$$E_a(\tau) = [\Delta G(\tau) + \lambda]^2/[4\lambda(\tau)], \quad (12)$$

which describe ETR along the vibrational and diffusion coordinates by introducing the τ-dependent pre-exponent and activation energy.

The dependence on τ can be described by the function φ(τ) needed to switch between the high-temperature

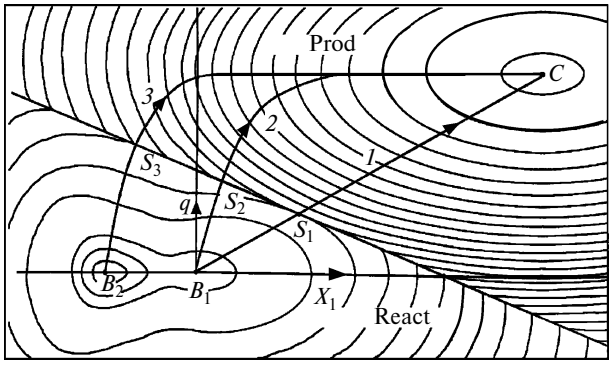

Fig. 11. Gibbs free energy surface for ETR from cytochrome heme *c*-559 to radical cation P^+ constructed within the framework of the combined two-mode model (data taken from Refs 74 and 75). The axes q and X correspond to the vibrational and diffusion coordinates of the reaction; React stands for reactants, Prod stands for products. For details, see text.

(nonadiabatic) and low-temperature (adiabatic) limits; therefore, $\varphi(\tau) \approx 1$ at room temperature and $\varphi(\tau) \ll 1$ at low temperatures. Then, the pre-exponent is represented by

$$\sigma(\tau) = k_0^{NA}[p_\sigma + (1 - p_\sigma)\varphi(\tau)], \quad (13)$$

where the parameter p_σ characterizes the contribution of the vibrational coordinate to the pre-exponent; therefore, the quantity $(1 - p_\sigma)\varphi(\tau)$ characterizes the contribution of the diffusion coordinate.

Analogously, the activation energy (12) is expressed through the τ-dependent rearrangement energy and the free energy of reaction:

$$\lambda(\tau) = \lambda[p_\lambda + (1 + p_\lambda)\varphi(\tau)], \quad (14)$$

$$\Delta G(\tau) = \Delta G[p_G + (1 + p_G)\varphi(\tau)], \quad (15)$$

where p_λ and p_G are the phenomenological parameters determining the temperature-independent contributions of the vibrational mode to λ and ΔG.

It should be noted that the numerator in expression (12) includes the total rearrangement energy λ corresponding to the high-temperature limit of expression (14) with $\varphi(\tau) = 1$. In the low-temperature limit one has

$$E_a(\tau) = (\Delta G p_G + \lambda)^2/(4\lambda p_\lambda), \quad (16)$$

where p_G and p_λ are less than unity. As a result, $E_a(\tau)$ increases as the temperature decreases.

Relations (11)—(15) were used to calculate the temperature dependences of the fractions of the reacted centers Q at different values of the parameters p_σ, p_λ, and p_G; the Q value is calculated[66] from the relation $Q = 1 - \exp(-k_{et}t_0)$, where $t_0 = 10$ μs. The ΔG_1, ΔG_2, and ΔG_3 values were set equal to −0.14, −0.18, and −0.29 eV, respectively. The best fit was obtained at $p_\lambda = 0.7$ and $p_G = 0.1$.

This approach allowed one to reasonably explain the temperature behavior of the empirical parameter Q used to characterize the rate of electron transfer for different cytochrome reduction states in the wide temperature range from 296 to 40 K (see Fig. 6). At the same time, this analysis was done assuming that the diffusion coordinate is characterized by one characteristic relaxation time τ; this precluded the explanation of the nonexponential behavior of the experimental[66] kinetic dependences.

Combined two-mode model. To obtain a complete description of all nonexponential kinetic curves of electron transfer in RC from *Rps. sulfoviridis* on the whole time scale in a wide temperature range at different degrees of reduction of cytochrome hemes, the model mentioned above was improved by using a combination of the Ovchinnikova—Sumi—Marcus and Rips—Jortner models.[74,75]

The function $F(t) = [P^+](t)/[P^+](0)$ describing the kinetic curves can be written as

$$F(t) = A_1 \int_0^\infty g(\tau) \exp[-k_{et}(\tau)t]dt + A_2 \exp(-k_r t), \qquad (17)$$

where $k_{et}(\tau)$ is the τ-dependent rate constant for the reaction and $g(\tau)$ is the Cole—Davidson function.

In expression (17), the integral and exponential terms describe the fast direct reaction $c\text{-}559^- \rightarrow P^+$ and the reverse reaction $P^+ \leftarrow Q_A^-$, respectively; for the coefficients A_1 and A_2, one has $A_1 + A_2 = 1$.

The integral term in expression (17) corresponds to the Rips—Jortner model if $k_{et}(\tau)$ is defined by relation (6). The authors of the model[61] reported that it allows one to correctly describe only the initial portions of the kinetic curves; this feature was used in our studies[74,76] and outlined above.

To describe the temperature behavior of the kinetic dependences on the whole time scale for different reduction states of cytochrome in a wide temperature range, we modified[74,75] expression (17) analogously to the empirical two-mode model.[57] Namely, $k_{et}(\tau)$ was defined by relations (11)—(15) in which the dependence on τ was introduced in the form

$$\varphi(\tau) = (1 + k_0^{NA}\tau/A)^{-1}, \qquad (18)$$

which, according to expression (6), serves to switch between the high-temperature (nonadiabatic, $\varphi(\tau) \approx 1$) and low-temperature (adiabatic, $\varphi(\tau) << 1$) limits.

Studies[74,75] were aimed to describe all available experimental curves (~50) in the temperature range 40—298 K for three reduction states of cytochrome in the RC from *Rps. sulfoviridis* within the framework of a unified model. In addition to the parameters appeared in relationships (1)—(3) for nonadiabatic electron transfer and the parameters used to describe electron transfer within the framework of an empirical two-mode model, the combined two-mode model includes the parameters β, τ_0, A_2, and k_r. It was assumed that the use of this model will be successfdul if the parameters p_σ, p_G and p_λ (they describe the distribution of the relaxation process between the vibrational and diffusion modes), the parameters β and τ_0 describing the dynamic behavior of the protein, and k_0^{NA} will be the same for all three reduction states of cytochrome.

The determination of these parameters is facilitated by the specific features of the kinetic curves studied. Initially, the parameters A_2 and k_r were determined for each curve using the semilogarithmic dependence on the time scale 100—4500 μs. Then, each curve was analyzed on the whole time scale using the integral ratio (17) at specified values of the parameters p_σ, p_G, and p_λ to determine the parameter β and the $k_0^{NA}\tau_0/A$ value by minimizing the standard root-mean-square deviation Φ. The k_0^{NA} values were also determined independently from the initial slope of the experimental curves taking into account the β values obtained. Then, the k_0^{NA} and $k_0^{NA}\tau_0/A$ values were used to calculate τ_0.

Finally, the parameters λ, ΔG, p_σ, p_G, and p_λ were varied in pair near their initial values under monitoring Φ. As a rule, the minimum Φ values were obtained at the parameter values taken from Ref. 73.

Analysis of the fast step of the kinetics of electron transfer. We calculated the kinetic curves of electron transfer using relations (11)—(15) and the parameters $p_\lambda = 0.7$ and $p_G = 0.1$ taken from Ref. 57. Computer simulation showed that these parameters give the best results. During computer simulation, the parameter p_σ took values in the range 10^{-3}—10^{-2}. The ΔG_1, ΔG_2, and ΔG_3 values are −0.14, −0.18, and −0.29 eV, respectively; for all reactions the values λ = 0.29 eV were taken from Ref. 73.

Using this approach, we described all experimental curves (~50) in the temperature range 40—298 K for three reduction states of cytochrome with high accuracy and determined the parameters characterizing electron transfer reactions in RC (see Figs 8 and 9). The parameters λ, ΔG, p_σ, p_λ, and p_G were the same and temperature-independent for all three degrees of reduction of cytochrome, whereas the parameters β and k_0^{NA} were temperature-dependent and obeyed the same temperature dependence for all three degrees of reduction of cytochrome (Fig. 12).

The parameter β characterizes the dielectric relaxation time distribution in the protein matrix where electron transfer occurs. This parameter indicates the relative contribution of the fast and slow degrees of freedom during dielectric relaxation of the protein. The β values obtained in our analysis are close to 0.04—0.06 for all three reduction states of cytochrome in the temperature range 298—220 K, which indicates a shift of the spectrum of diffusion motions to the high-frequency region. At 200—130 K, β increases from 0.08 to 0.2 and reaches a value of 0.57 at 40 K.

The parameter $k_0^{NA}\tau_0/A$ characterizes the degree of adiabaticity of the reaction. For the RC containing cytochrome in the first reduction state, $k_0^{NA}\tau_0/A = 10$ at room temperature and increases to 178 as the temperature decreases to 219 K. It follows that even at room temperature, ETR are adiabatic for the fraction of proteins with longest relaxation times. At the same time, for most proteins one has β = 0.05 at room temperature and the average relaxation time $\tau_{av} = \beta\tau_0$ ensures the nonadiabaticity of the reaction. As the temperature decreases, both τ_0 and β increase; consequently, the degree of adiabaticity increases.

In the course of analysis, k_0^{NA} is determined as independent parameter equal to $1.4 \cdot 10^7$ s^{-1} at room temperature for all three reduction states of cytochrome. If k_0^{NA} is known and it is possible to estimate the A value (assuming $\varepsilon_s/\varepsilon_\infty = 2$ and λ = 0.29 eV), one gets $\tau_0 = 0.35$ μs at room temperature. As a result, for the average relaxation time in

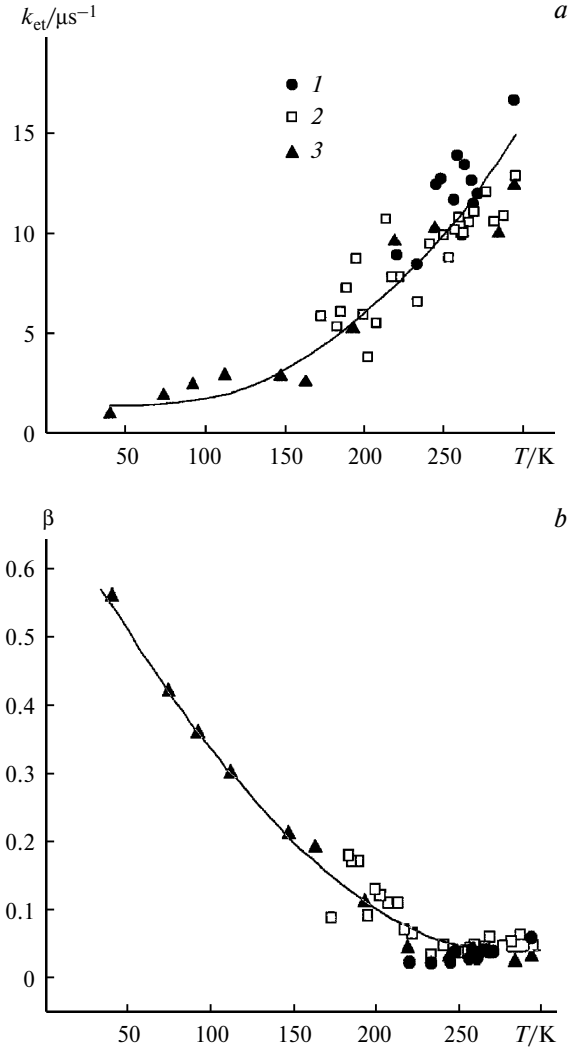

Fig. 12. Temperature dependences of parameters k_0^{NA} (*a*) and β (*b*) determined using the combined two-mode model for the first (*1*), second (*2*), and third (*3*) reduction states of cytochrome.

the protein one has $\beta\tau_0 = 17.5$ ns. This is in reasonable agreement with the relaxation time of the myoglobin heme envelope (9 ns) measured by recording the relaxation shift of the fluorescence spectrum of the dye incorporated into the myoglobin heme envelope.[35] The τ_0 and β values obtained at lower temperatures are also close to the values of analogous parameters determined by Mössbauer spectroscopy for the heme dynamics in myoglobin.[43]

Analysis of the slow phase of the kinetics of electron transfer. A detailed analysis showed that the intergral term in expression (17) describes only the initial portions of the kinetic curves in time interval 0.1—40 μs. At $t > 40$ μs, the contribution of the integral part of this equation is negligible and all kinetic curves are well described by the exponential term $A_2\exp(-k_b t)$ with $k_b = (1—4)\cdot 10^2$ s^{-1}.

This behavior of the kinetic curves can be explained assuming the presence of two protein populations in the sample. The first population is characterized by fast electron transfer from the reduced heme *c*-559$^-$ to P^+ with $k_{et} = 10^7—10^4$ s^{-1}. The kinetics of electron transfer in this population is described by the parameters given above and the contribution of the reverse reaction $P^+ \leftarrow Q_A^-$ in the reduction of P^+ in this population is negligible. In the second population, one has $k_{et} << 10^2$ s^{-1} for the direct reaction and the reduction of P^+ is due to the reverse reaction. The parameters A_1 and A_2 are coefficients corresponding to the fractions of the "fast" and "slow" protein populations. A similar conclusion about the existence of equilibrium between two states of the cytochrome—RC complex, active and inactive with respect to the direct electron transfer to P^+, was formulated earlier[64,88] and discussed in Refs 66 and 68.

Nevertheless, two questions remained unsettled.

1. What is the reason for so large differences in the kinetics of direct electron transfer between the "fast" and "slow" protein populations?

2. What is the reason for changes in the parameters A_1 and A_2 (describing the equilibrium between two populations of the cytochrome—RC complex) as a function of temperature and the reduction state of cytochrome?

For the first reduction state of cytochrome a transition from the "fast" to "slow" population occurs with an activation energy of 0.22 eV.[74] For the third reduction state of cytochrome, the activation energy is only 0.031 eV. What is the reason for such a large change in the equilibrium between two types of protein complex during the reduction of cytochrome?

In this study we assumed the possibility of coexistence of two different states of proteins, B_1 and B_2, with small difference in the free energy of the initial state of electron transfer (see Fig. 11). Since A_1 and A_2 appear to be dependent on temperature and on the degree of reduction of cytochrome hemes, the free energy difference between these two states should be comparable with the energy of thermal motion and the energy of electrostatic interaction between charges attached to the proximal heme of cytochrome and the extra electrons attached to the neighboring hemes. From ΔG values[57,74—76] it follows that this energy difference should be 0.04—0.15 eV.

The dependence of the free energy difference between the protein states B_1 and B_2 on the reduction state of the cytochrome hemes *c*-552 and *c*-556 separated from the heme *c*-559 by 14 and 27 Å, respectively, means that proteins in these states have different charge distribution in the vicinity of the proximal heme. Physically, this can be due to protonation of the amino acid residue near the proximal heme with an activation energy of 0.1—0.2 eV.

For instance, a carboxyl group near the proximal heme can be in the deprotonated state at room temperature and in the protonated state at lower temperatures. In the first reduction state of cytochrome, the negatively charged carboxylate ion creates favorable energy conditions for fast

electron transfer from the state B_1 to the final state C along pathway *1* (room temperature, $k_{et} \sim 10^7$ s^{-1}) or along pathway *2* (220 K, $k_{et} = 10^4$ s^{-1}) (see Fig. 11). At low temperatures, the carboxylate ion is protonated due to proton diffusion with characteristic times $\tau >> 10^{-2}$ s in the interior of the protein globule; this causes transition of the protein to the state B_2 with lower electron energy. The system can go from the state B_2 to the final state C along pathway $B_2 \Rightarrow B_1 \Rightarrow C$ (pathway *2*) or directly from B_2 to C (pathway *3*) with a much higher activation energy (see Fig. 11). The rate of electron transfer from B_2 to C along pathways *2* and *3* is less than 10^2 s^{-1}.

In the reduction of the heme *c*-556 the equilibrium is shifted toward the deprotonated state owing to electrostatic interaction of this heme with the proton of carboxyl groups. As a result, the rate of electron transfer at a given temperature increases and the reaction can be observed at lower temperatures. Attachment of the third electron to the heme *c*-552 causes even larger displacement of H^+ from the carboxyl group. Thus, the deprotonation state becomes more pronounced and electron transfer remains fast at the lowest temperatures. As can be seen from the experimentally determined temperature dependence of the ratio A_1/A_2 (see Ref. 74), the equilibrium between the nonprotonated state B_1 and protonated state B_2 is characterized by a free energy difference of 0.22 eV for the first reduction state of cytochrome and 0.031 eV for the third reduction state. The free energy increment equal to 0.19 eV is in good agreement with the difference $\Delta G_1 - \Delta G_3 = 0.15$ eV corresponding to the electrostatic contribution to the increase in the rate of electron transfer in "fast" protein complexes as was used in our model.

According to conventional nonadiabatic or adiabatic approximation, a decrease in ΔG due to electrostatic interaction by 0.1—0.2 eV at $\lambda = 0.29$ eV can not be a reason for changes in k_{et} by four and more orders of magnitude. Such large changes in the electron transfer rate can be explained within the framework of the two-mode model by the changes in the relative contributions of the vibrational and diffusion degrees of freedom to the parameters λ and ΔG according to expressions (11)—(15). Combining various contributions of temperature-independent vibrational and temperature-dependent diffusion mode to protein reorganization makes it possible to explain a great difference between the rates of ETR in proteins (four and more orders of magnitude).

Thus, within the framework of this model it is possible to analyze the regularities of changes in the kinetics of the fast component and in the relative contributions of the fast and slow components of the reduction reaction of P^+ in the RC on variation of the temperature and the degree of reduction of cytochrome. The analysis allows one to quite accurately describe this reaction using a broad dielectric relaxation time distribution in the protein structure. Separation of the relaxation process in proteins into two types characterized by different activation parameters helps to effectively control the electron transfer rate in organized molecular systems within the limits of four and more orders of magnitude.

However, the proposed combined two-mode model does not allow one to relate the values of its empirical parameters to a particular structure of the protein globule, although it describes all types of kinetic curves in a wide temperature range with high accuracy (see Figs 8 and 9). This strongly reduces the possibility of analysis of electron transfer in various proteins and to a great extent reduces the predictive power of the model.

To provide a more complete account of the quantum and dynamic effects in ETR in protein globules, the following modification of the model was proposed.

The OGSM model. *Description of the model.* Within the framework of the empirical combined two-mode model (see above) electron transfer began at particular point B on the two-dimensional surface and proceeded by the motion along the vibrational and diffusion coordinates to the final point C (see Fig. 11) The diffusion dynamics of the medium was specified by the Cole—Davidson distribution to describe the nonexponential behavior of the kinetic curves observed.

A better physical description of the process can be obtained using the Ovchinnikova—Gelman—Sumi—Marcus model (OGSM)[84,87,89] which assumes that at the initial point B there exists a Gaussian energy distribution along the diffusion coordinate X, the dielectric relaxation of the protein is described by the classical equation of diffusion along the coordinate X, and a reaction along the vibrational coordinate q is possible (Fig. 13). Then, at high temperatures, electron transfer goes along trajectory *1* to point D with the minimum activation energy due to fast diffusion. As temperature decreases, the population at the point D decreases owing to the change in the width of the

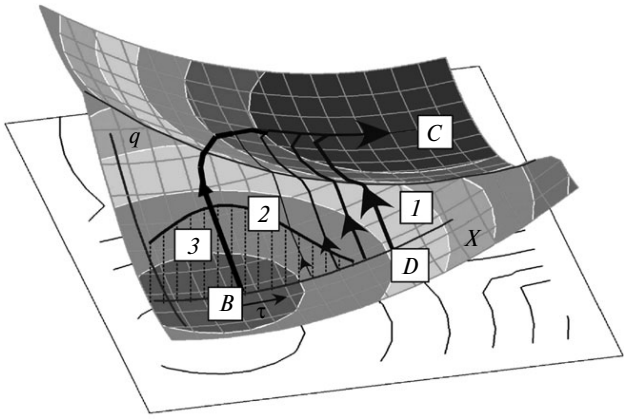

Fig. 13. Gibbs free energy surface for ETR constructed within the framework of the OGSM model (data taken from Refs 77—79). The axes q and X correspond to the vibrational and diffusion coordinates of the reaction. For details, see text.

distribution and retardation of diffusion along the coordinate X; this allows competing reactions to proceed along other trajectories (trajectory *2*). At the lowest temperatures (either under slow diffusion conditions or with no diffusion), reactions at strongly different rates are possible at different X values (including trajectory *3*); this leads to a wide reaction rate distribution even if diffusion along the coordinate X is characterized by a single time τ (no relaxation time distribution).

This model was introduced, first, to obtain a full description of the kinetics of electron transfer in the temperature range from ambient to helium temperatures; this requires a joint consideration of the effect of dielectric relaxation of the protein and vibrational quantum effects on the transfer rate. Second, based on the developed model for electron transfer, it was assumed to determine general parameters of this process including the characteristic times of diffusion along the coordinate X and their temperature dependences.

This model is described by the classical diffusion equation with the response[90,91] for the distribution function $P(X;t)$:

$$\frac{\partial P}{\partial t} = \frac{k_B T}{\tau}\frac{\partial^2 P}{\partial X^2} + \frac{1}{\tau}\frac{\partial}{\partial X}\left(P\frac{dV}{dX}\right) - k(X)P, \qquad (19)$$

where $V(X) = 0.5X^2$ is the harmonic potential along the diffusion coordinate for reactants and the reverse reaction is ignored.[84,92]

At a given X, the rate constant is given by[93]

$$k(X) = \frac{V_{ab}^2}{h}\sqrt{\frac{\pi}{\lambda_2 k_B T}}\exp\left\{-\frac{[\lambda_1 + \Delta G(X)]^2}{4\lambda_2 k_B T}\right\}. \qquad (20)$$

The relaxation spectrum of the protein includes three modes, *viz.*, a slowly relaxing diffusion mode X (frequency ω_X, reorganization energy λ_X) and two rapidly relaxing modes, a "quantum" intramolecular mode (ω_q,λ_q) and a "classical" mode (ω_{c_l},λ_{c_l}). The former specifies the dependence of the driving force on X

$$\Delta G(X) = \Delta G^0 + \lambda_X - X\sqrt{2\lambda_X},$$

and last two modes are responsible for the parameters $\lambda_1 = \lambda_q + \lambda_{c_l}$ and

$$\lambda_2 = \frac{h\omega_{cl}\lambda_{cl}}{2k_B T}\,\mathrm{cth}\left(\frac{h\omega_{cl}}{2k_B T}\right) + \frac{h\omega_q\lambda_q}{2k_B T}\,\mathrm{cth}\left(\frac{h\omega_q}{2k_B T}\right).$$

The role of quantum vibrational effects in ETR was studied in detail.[50,91,94—97] In the classical theory,[51] the rate of electron transfer rapidly tends to zero as temperature decreases except a rare case of a barrierless process. Vibrational quantization leads to a finite reaction rate which is temperature-dependent at $T < h\omega/(2k_B)$, where ω is the frequency of the vibrational mode of the acceptor. The values reported for the protein structures including RC of photosynthetic bacteria are $\omega = 240$,[95] 300—400,[91] and 400—800 cm^{-1}.[96]

The original model included only the modes X and q, but we found[77—79] that the description of the temperature dependence of the reaction kinetics in the high-temperature region $T > h\omega_{c_l}/(2k_B)$ requires the inclusion of the classical low-frequency mode with high reorganization energy. To reproduce the behavior of the curves at low temperatures, we assume that the "classical" modes ω_X and ω_{c_l} become quantum ones at $T < T_g$. The classical modes correspond to two types of dipole relaxation of the medium, *viz.*, fast relaxation related to, *e.g.*, free reorientation of water molecules and amino acid residues, and slow relaxation hindered by reorientations, which is described by a stochastic process in accordance with expression (19).

Equation (19) can be solved with the initial condition

$$P(X;0) = \frac{1}{\sqrt{\pi\hbar\omega_X\,\mathrm{cth}[\hbar\omega_X/(2k_B T)]}}\cdot \exp\left\{-\frac{X^2}{\hbar\omega_X\,\mathrm{cth}[\hbar\omega_X/(2k_B T)]}\right\},$$

which also takes into account the quantum character of the mode X at low temperatures. Numerical solution was found by expansion over the eigenfunctions of the diffusion operator (they are the same as those of the harmonic oscillator);[98] convergence was attained with ten basis functions. In the experiments, the population of the initial state is measured:

$$Q(t) = \int_{-\infty}^{\infty} P(X;t)\,dX. \qquad (21)$$

For the fast and slow diffusion limits, the population is given by expressions (22) and (23), respectively.

$$Q(t) = \exp(-k_e t) \qquad (k_e\tau << 1) \qquad (22)$$

$$Q(t) = \int_{-\infty}^{\infty} P(X;0)\exp[-k(X)t]\,dX \qquad (k_e\tau >> 1) \qquad (23)$$

Within the framework of this model we analyzed the electron transfer reactions in RC;[77—79] successively analyzed the kinetics of electron transfer between the proximal heme of cytochrome *c*-559 and the bacteriochlorophyll dimer P in two different types of RC isolated from bacteria *Rps. viridis* and *Rps. sulfoviridis*, as well as in seven mutant-modified RC isolated from the photosynthetic bacteria *Rps. viridis* in which the amino acid tyrosine L162 (Y) located at the midpoint of transfer pathway between c-559$^-$ and P^+ (see Fig. 7) was replaced by phenylalanine (F), tryptophan (W), glycine (G), methionine (M), leucine (L), threonine (T), or histidine (H). Studies were carried out in the temperature range 298—8 K for the native and mutant RC from *Rps. viridis* and in the temperature range 298—40 K for the RC from *Rps. sulfoviridis*.

According to X-ray data, there is a number of water molecules near the trajectory of electron transfer in the protein from *Rps. viridis*; one molecule, HOH38, is located near the heme *c*-559 (see Fig. 7).[46]

Clearly, even minor changes in the structure of the amino acid residue can affect the squared matrix element V_{ab}^2, change the local polarity in this region of the protein structure and thus the reorganization energy and the probability of incorporation of the water molecule HOH38 into the RC; this to a great extent determines the rate of electron transfer.

As an example of application of the OGSM model to analysis of experimental data, Fig. 14 presents a family of experimental curves obtained at different temperatures for the mutant derivative RC L162T and the results of their simulation within the framework of the model proposed.

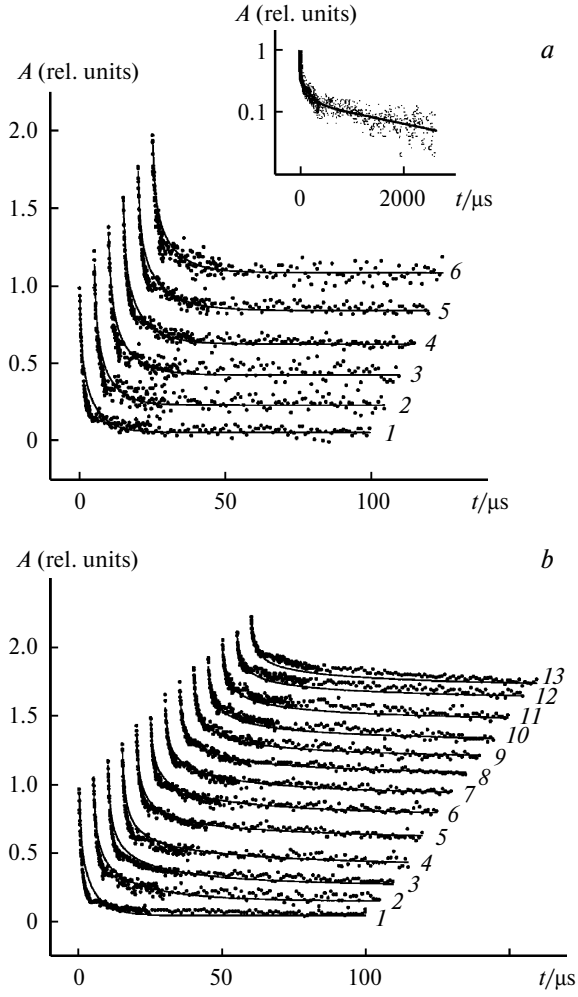

Fig. 14. Experimental kinetic curves of mutant L162T (points) obtained in the high-temperature (*a*, T = 295 (*1*), 288 (*2*), 278 (*3*), 268 (*4*), 256 (*5*), and 246 K (*6*)) and low-temperature (*b*, T = 293 (*1*), 237 (*2*), 220 (*3*), 203 (*4*), 182 (*5*), 159 (*6*), 140 (*7*), 120 (*8*), 102 (*9*), 80 (*10*), 60 (*11*), 38 (*12*), and 10 K (*13*)) series of measurements and their theoretical approximations (solid lines). Inset: data for T = 182 K (see Ref. 79); A is the absorbance of P^+.

Choice of parameters. The model includes one dynamic parameter τ whose dependence on T should be determined, and a number of temperature-independent static parameters determining $k(X)$. The modes of the medium are assumed to be classical at $T > T_g$ and quantum at low T; the numerical value chosen was $\omega_{cl} = \omega_X = 2T_g \approx 250$ cm^{-1}, this gave the best result in the low-temperature region. The other six static parameters, namely, V_{ab}, ΔG°, ω_q, λ_q, λ_{cl}, and λ_X, appear in expression (20) as four combinations. It follows that the model does not allow one to exactly determine all static parameters because variation of parameters at constant values of the combinations (see above) does not affect the quality of the fit of theoretical to experimental curves. Therefore, two parameters can be fixed. The intramolecular mode is considered quantum at all temperatures; its frequency was set to $\omega_q = 800$ cm^{-1}. The ΔG values used were $\Delta G_1 = -0.14$ eV, $\Delta G_2 = -0.18$ eV and $\Delta G_3 = -0.29$ eV, as was determined earlier.

Among the other four parameters, two can be chosen based on the condition for equal slopes of the initial portions of the theoretical and experimental curves at ambient and low temperatures (in accordance with expressions (22) and (23)); therefore, one gets only two arbitrarily varied parameters. By varying them and τ a minimum standard deviation of the experimental curve from the calculated one was determined and thus the τ value for a given temperature was found. At $T > T_g$, the function $\tau(T)$ thus obtained was represented as

$$\tau(T)^{-1} = \tau_\infty^{-1}\exp[-E_a/(k_B T)]. \qquad (24)$$

More detailed description of the procedure for the choice of parameters and determination of $\tau(T)$ can be found in Ref. 77.

By analogy with the combined two-mode model that includes the relaxation time distribution, the initial processing of experimental data involved determination of the relative population A_s and the rate constant k_s for the slow population using the portion of the curve at $t > 100$ μs,[77–79] as shown by the solid line in the inset in Fig. 14, *a*. In simulating the total kinetic curve $Q_{theor}(t)$ the contribution of the fast population was assumed to be proportional to $1 - A_s$; therefore, the kinetic curve was represented by

$$Q_{theor}(t) = (1 - A_s)Q(t) + A_s\exp(-k_s t), \qquad (25)$$

where $Q(t)$ was calculated as described above.

Thus, in the course of analysis using this model the static parameters $\omega_{cl} = \omega_X = 2T_g \approx 250$ cm^{-1}, $\omega_q = 800$ cm^{-1}, $\Delta G_1 = -0.14$ eV, $\Delta G_2 = -0.18$ eV and $\Delta G_3 = -0.29$ eV were specified based on the published data, they had the same values, and were considered as temperature-independent for all types of RC. Simulation of the kinetic curves gave

the parameters V_{ab}, λ_q, λ_{c_l}, and λ_X of each protein (they also were independent of temperature and of the degree of cytochrome reduction) and the temperature-dependent average relaxation time of the protein τ, which characterizes its mobility. Finally, all key factors governing the kinetics of electron transfer in the native and mutant proteins in the temperature range from ambient to helium temperatures were determined and analyzed.

Analysis of static parameters. The static parameters V_{ab}, λ_q, λ_{cl}, and λ_X characterizing the rate of the reaction in a given conformation X are temperature-independent. Table 1 lists their values for all proteins; they were found by computer simulation of the kinetic curves.

The numerical value of the matrix element V_{ab} is given in Table 1. This key parameter determines the overlap of the donor and acceptor wavefunctions and thus the exponential dependence of the electron transfer probability on distance. The V_{ab} magnitude can change significantly (to 40 times) upon replacement of amino acids on the pathway of electron transfer. Taking into account the fact that the expressions (2) and (20) for the rate constant include the squared V_{ab}, changes in this parameter only can change $k(X)$ by more than three orders of magnitude.

The matrix element of electron transfer in photosynthetic bacterium *Chromatium* was reported to be $V_{ab} = 3\ cm^{-1}$ (the electron transfer distance was estimated as $R = 8$—10 Å between the outermost points)[95] and 0.1—0.4 cm^{-1} (R = = 12—13 Å),[96] which is comparable with the data of Table 1. One can also compare the obtained value V_{ab} with the empirical formula[99] which predicts a linear dependence of $\log_{10}V_{ab}^2$ on ρ (fraction of the space between the donor and acceptor which is occupied by atoms)

$$\log_{10}V_{ab}^2 = \log_{10}V_{ab_0}^2 - (1.2 - 0.8\rho)(R - 3.6), \qquad (26)$$

where R is the distance between the outermost points of electron transfer in Å and V_{ab_0} is the value of the matrix element in the case of direct contact (R = 3.6 Å). We calculated ρ for a structural fragment of a RC, confined within a cylinder 4 Å in diameter and 8.5 Å long, whose axis passes through the iron ion of the heme *c*-559 and the Mg ion of the special pair in the subunit L. The results of calculations for all studied RC in the form of the dependence of the decimal logarithm of the squared matrix element on ρ at constant R are shown in Fig. 15. As can be seen, the data of Table 1 for the wild strain and mutants *Rps. viridis* agree with the results obtained from expression (26) at $V_{ab_0} = 10^3\ cm^{-1}$. The large V_{ab_0} value means that at tight contact the reaction is adiabatic on the whole time scale and its rate reaches a maximum value of $10^{13}\ s^{-1}$ predicted by the transition state theory for barrierless reactions and also included in the empirical formulas for the reaction rate.[54,55,99] A fairly large scatter of points in Fig. 15 may indicate a conditional character of the parameter ρ proposed in Ref. 99. A more rigorous theory, which can explain the dependence of the matrix element on the chemical nature of the protein medium along the pathway of electron tunneling was reported elsewhere.[100]

From Table 1 it follows that the total reorganization energy λ varies within 0.4—1 eV; in particular, λ = 0.9 eV for the wild strain *Rps. viridis*, which agrees with the published data[51,99,101] (0.6—0.8 eV). The reorganization energy along the conformational coordinate λ_X varies from 0.09 to 0.22 eV, being equal to 0.09 eV for the wild strain; this agrees with a value of 0.07 eV obtained for *Rps. viridis*.[102] Microscopic calculations of the reorganization energy corresponding to electron transfer between two cytochromes *c* in the protein matrix carried out using X-ray

Table 1. Static parameters of the model for the native RC and mutants L162X *Rps. viridis*

X	V_{ab}/cm^{-1}	λ_a	λ_X	λ_{cl}	λ*
		eV			
F	1.1	0.035	0.22	0.66	0.92
G	0.2	0.020	0.19	0.31	0.52
M	3.4	0.039	0.09	0.89	1.02
L	0.2	0.022	0.20	0.34	0.56
W	1.5	0.034	0.21	0.64	0.88
T	0.08	0.015	0.19	0.19	0.40
H	1.5	0.033	0.12	0.69	0.84
Y**	2.2	0.035	0.09	0.77	0.90
*R.s.***	0.25	0.010	0.20	0.22	0.43

* The total reorganization energy.
** Wild strain *Rps. viridis*.[77]
*** *Rps. sulfoviridis*, reduction state *2*.[78]

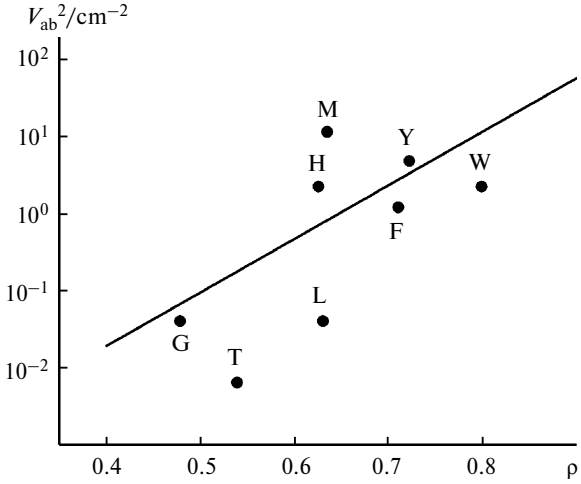

Fig. 15. Squared electron matrix element V_{ab}^2 (filled circles denote data from Table 1) plotted *vs.* fraction of space between electron donor and acceptor; this space is occupied by atoms and varies upon replacement of the amino acid in position L162. Straight line represents the results of calculations using expression (26) at $V_{ab_0} = 10^3\ cm^{-1}$. The transfer distance between the outermost points is assumed to be equal for all strains: R = 12.3 Å.

structural data for the protein gave $\lambda = 9$—15 kcal mol^{-1} ≈ ≈ 0.39—0.65 eV for the total reorganization energy[103] and $\lambda_q = 1$ kcal mol^{-1} ≈ 0.043 eV for the energy of intramolecular reorganization.[104] Our results qualitatively agree with the cited data, also with respect to the small λ_q value.

Analysis of the temperature dependences of τ. Our analysis showed that the dynamic parameter τ is strongly dependent on temperature; its value was determined for all kinetic curves by computer simulation. As an example, Fig. 16 presents the temperature dependence of τ for L162T in the coordinates $1/T$, $\log_{10}\tau$; the straight line is an approximation using expression (24). The activation energies E_a (eV) obtained taking into account the slopes of the straight lines for all native and mutant RC L162X from *Rps. viridis* are listed below.

X	Y	F	G	M	L	W	T	H	*Rps. sulfovir.**
E_a/eV	0.50	0.23	0.22	0.09	0.30	0.27	0.15	—	0.05

* RC from *Rps. sulfoviridis.*

The activation energy thus determined for the native RC from *Rps. viridis* is $E_a = 0.5 \pm 0.1$ eV, as derived from experiments carried out in 66% glycerin solution.[77] This value is equal to the activation energy of relaxation dipole rearrangement of viscous glycerin (66%) surrounding triplet excited eosin dye. In this case, the relaxation times were determined from the instantaneous phosphorescence spectra of the dye.[105] One could assume that the molecular dynamics of the protein globule is mainly determined by the solvent dynamics. However, the values obtained in analogous experiments with RC from *Rps. sulfoviridis* appeared to be much lower (0.05—0.1 eV).[78] Such a large difference between two proteins with similar properties reqiured an explanation. A possible reason for the large difference in the activation energies between RC from *Rps. viridis* and *Rps. sulfoviridis* can be associated with changes in the network of hydrogen bonds caused by the presence of water molecule near the heme *c*-559.

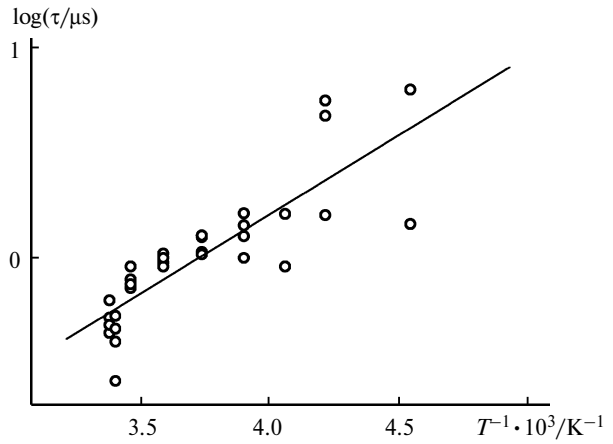

Fig. 16. Decimal logarithm of the relaxation time τ determined from the minimum of the standard deviation of the theoretical curves from experimental ones plotted *vs*. inverse temperature for L162T. Straight line represents approximation using expression (24) at $T > T_g \approx 180$ K.

The structure of RC from *Rps. viridis* (1PRC in Brookhaven Protein Databank)[47] contains a water molecule HOH38 in the vicinity of the heme *c*-559 (W1, see Fig. 7). Based on the interatomic distances and bond angles, HOH38 can form four hydrogen bonds (two bonds as proton donor and two bonds as proton acceptor). High E_a value for *Rps. viridis* can mean that the relaxation process includes cleavage of some hydrogen bonds of this molecule. Small E_a value for *Rps. sulfoviridis* possibly implies the absence of HOH38 in the RC structure.[77]

By analogy one can assume that variation of E_a in the range 0.15—0.30 eV among the mutant RC from *Rps. viridis* is due to the change in the number of hydrogen bonds formed by this molecule with the environment or to the change in the number of water molecules. In Ref. 106, the structures L162F and L162T in the region between *c*-559 and P were shown. It was stated that all structural differences between these mutants and the wild strain are located within the mutation site; however, the molecule HOH38 in the heme *c*-559 is not seen, probably, because of the choice of projection. The activation energies of 0.23 eV (L162F) and 0.15 eV (L162T) could indicate that the position of this molecule changed in the sense that the number of hydrogen bonds decreased or they have weakened compared to the wild strain (L162F). Another explanation suggests the absence of HOH38 molecule (L162T); but to prove this suggestion, accurate structural data are needed. Unfortunately, this information was not reported and is now unavailable*.

Analysis of occupancy of the slow population of RC. Similarly to the preceding model, an analysis of experimental data shows that the amplitude of the inert population A_s abruptly increases as temperature decreases. Based on the observed temperature dependence, one can assume that the active and inert populations represent two states of the protein with different energy and entropy values, which coexist in thermodynamic equilibrium until application of a laser pulse. Having designated the corresponding differences as ΔE and ΔS, the temperature dependence of A_s can be represented as follows:

$$A_s = \left[1 + \exp\left(\frac{T\Delta S - \Delta E}{k_B T}\right)\right]^{-1}. \qquad (27)$$

The dependences of $\log_{10}[(1 - A_s)/A_s]$ on $1/T$ for RC from *Rps. sulfoviridis* for three degrees of reduction of the cytochrome hemes are shown in Fig. 17. The parameters of approximation of experimental data by the Arrenius dependences for all native and mutant RC are listed in

* J. Wachtveitl, D. Oesterhelt, private communication.

Table 2. If we additionally assume that two populations differ in protonation state of a particular group of the protein, one can calculate pK_a of this protonated group using the expression

$$pK_a = pH - (T\Delta S - \Delta E)/(k_B T \ln 10).$$

The pK_a values are also listed in Table 2. As can be seen, mutations have little effect on the pK_a values of this hypothetical group for all studied native and mutant proteins (most of them are equal to 6.6±0.2 at pH = 8.0 and 294 K). As temperature decreases, the equilibrium is significantly shifted in accordance with activation energies determined for different RC. This will lead to a change in the potential near the donor or acceptor center. At the same time, from the experiment on RC from *Rps. sulfoviriids* one can see that the equilibrium is also strongly dependent on the degree of reduction of cytochrome hemes (see Fig. 17, Table 2). This means that the hypothetical group is located near the cytochrome hemes, probably, near the heme *c*-559 exhibitng electron-donating properties. From the data of Table 2 it follows that for the RC from *Rps. sulfoviridis* the activation energy for the first, second, and third degrees of reduction of cytochrome for the dependence of $\ln_{10}[(1 - A_s)/A_s]$ on $1/T$ is equal to 0.25, 0.16, and 0.04 eV, respectively; this is in excellent agreement with the corresponding values obtained[74] within the framework of the combined two-mode model.

Conclusions

Experimental data outlined in the present review and their analysis show that electron transfer in proteins obeys general regularities of electron transfer in the condensed phase provided that specific features of the protein molecules as highly organized nanostructures are taken into account appropriately. Moreover, in some cases proteins can act as model systems to facilitate the setting and interpretation of such experiments, because positions of the donor and acceptor centers and atoms between them in the proteins with known atomic structure were determined with high accuracy; experiments in solution or in polymer matrices often have a drawback related to uncertainty in determining atomic positions.

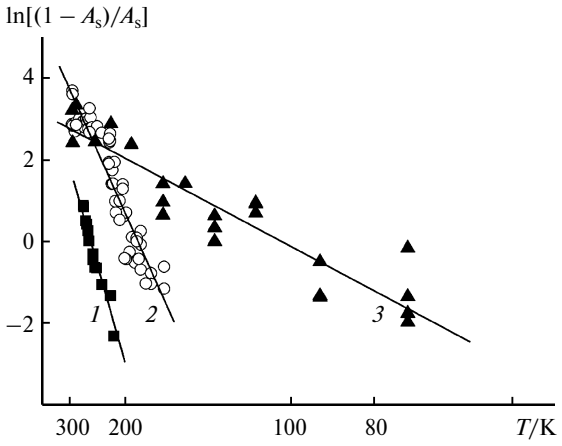

Fig. 17. Arrhenius plots of the parameter $\ln(1 - A_s)/A_s$ characterizing the ratio of the "fast" and "slow" populations of the protein complexes of RC from *Rps. sulfoviridis* for different reduction states of cytochrome hemes: only heme *c*-559 is reduced (*1*), hemes *c*-559 and *c*-556 are reduced (*2*), and hemes *c*-559, *c*-556, and *c*-551 are reduced (according to data taken from Ref. 78).

Table 2. Parameters of the inert population in native RC and mutants L162X *Rps. viridis*

X	ΔE/eV	ΔS/meV K^{-1}	pK_a
F	0.14	0.76	6.5
G	0.13	0.74	6.5
M	0.12	0.70	6.6
L	0.10	0.59	6.8
W	0.11	0.69	6.6
T	0.08	0.56	6.5
H	0.09	0.60	6.5
Y*	0.19	1.0	6.0
1**	0.25	0.98	7.3
2**	0.16	0.84	6.4
3**	0.04	0.36	6.8

* Wild strain[77].

** **1**—**3** are *Rps. sulfoviridis*[78] in the reduction states *1*, *2*, and *3* of cytochrome: only the heme *c*-559 is reduced (*1*), the hemes *c*-559 and *c*-556 are reduced (*2*); and the hemes *c*-559, *c*-556, and *c*-552 are reduced (*3*). The mutants and wild strain *Rps. viridis* were studied in the state *2*.

Now we can summarize the available data on the conductivity of the protein globule which are characterized by dependences of the rate constant for electron transfer k_e on the distance R or on the structure of the protein matrix separating the electron-transfer centers. A conclusion can be made that proteins, as polypeptide structures, exhibit no increased conductivity. Two models, namely, the model of tunneling over the shortest distance through a protein as isotropic barrier taking into account its close packing by the side amino acid residues[99] or tunneling along the polypeptide chain due to superexchange interaction involving σ-bonds and hydrogen bonds of the protein,[10,13,14,19,58] give nearly equal accuracy of estimates, and at present it is impossible to make an unambiguous choice between them. A more strict theory which explains the dependence of the matrix element on the chemical nature of the protein medium along the pathway of electron tunneling is available;[100] unfortunately, it was used to analyze only a few experimental data.

High efficiency of long-range electron transfer in protein structures over distances of the order of tens and hundreds of Ångstrøms is ensured by sequential transfer of single electrons between metal-containing centers over dis-

tances 5—15 Å, which takes time from 10^{-10} to 10^{-5} s. Assuming that traveling a distance of 5 Å in a protein takes 10^{-10} s, one can readily calculate that electrons will move at a velocity of 50 m s^{-1}. If an electron is transferred over a distance of 15 Å in 10^{-5} s, the electron velocity is 0.15 m s^{-1} (*cf.* about 0.1 m s^{-1} for conventional metallic conductors). Assuming that a single electron is localized on a small 20-Å metal-containing protein (*e.g.*, cytochrome *c*), the first estimate suggests passage of a total of $2.5 \cdot 10^9$ electrons per second along the chain of close-packed proteins. At a protein molecule cross section of 400 $Å^2$, this corresponds to a current density of 100 A mm^{-2} and much exceeds the conductivity of the best conductors.

At the same time, analysis of experimental data presented in this review shows that the efficiency of electron transfer to a great extent depends on the nature and rate of relaxation processes in the protein, which in turn are determined by the structure and dynamics of the protein globule. The models considered above to different extent take into account these features of proteins.

The results obtained indicate that the OGSM model, which allows a protein to relax involving both quantum vibrational and diffusion degrees of freedom, correctly describes the kinetics in a wide temperature range from ambient to helium temperatures. Slow reorientation of molecular dipoles introduces adiabaticity into the reaction that was initially nonadiabatic owing to a long distance between the donor and acceptor. As a result, the effect of the protein dynamics manifests itself in that the reaction proceeds by the nonadiabatic mechanism on the short-time scale and by the adiabatic mechanism on the long-time scale, so the final stage of the reaction is controlled by the protein dynamics. Owing to the quantum nature of vibrations with frequencies of the order of $2k_BT_g/h$, the reaction rate at $T < T_g$ remains fairly high compared to the initial reaction rate; this allows one to reproduce the behavior of the experimental kinetic curves at low temperatures within the framework of the OGSM model.

The data of Table 1 indicate that, within the framework of the OGSM model, the adiabaticity parameter η is large for all RC studied even at room temperature. For instance, assuming the minimum reorientation time of molecular dipoles to be $\tau = 0.1$—0.5 μs for all mutants (for L162T, see Fig. 16), one gets $\eta = 75$—2.5; as temperature decreases, η increases due to an increase in τ. This agrees with the conclusion following from the analysis performed within the framework of the combined two-mode model; also, it supports the conclusions[56] that reactions of electron transfer over distances of 12—14 Å proceeding on the microsecond time scale should be considered in the adiabatic approximation.

Two circumstances confirm the main conclusion about strong effect of protein dynamics on electron transfer from *c*-559 to P^+ which was based on the model proposed. These are a minimum in the dependence of the standard deviation of the calculated kinetic curves from the experimental data on τ and good agreement between theoretical with experimental curves in a wide temperature range from ambient to helium temperatures provided an appropriate choice of τ for each curve (see Fig. 14). It should be emphasized that this was attained using a few arbitrarily varied fitting parameters. In fact, only one temperature-dependent dynamic parameter τ was chosen individually for each curve. Among eight static temperature-independent parameters, four (three vibrational frequencies and the driving force of the reaction) were chosen to be equal for all RC and their values were fixed. Two other parameters , a combination of the matrix element of electron transfer and the reorganization energies on three modes, were chosen for each RC from the initial slopes of the experimental curves at high and low temperatures. Only two remaining parameters were fitting ones because they were arbitrarily varied to obtain the best results. Experiment gives a complex nonexponential kinetics even at high temperatures; therefore, reproduction of the kinetic behavior in wide temperature range using a few fitting parameters counts in favor of the model proposed.

Simulation of the kinetic curves for RC from *Rps. viridis* (wild strain)[77] and *Rps. sulfoviridis*[78] appeared to be successful due to the assumption of classical vibrations ($\omega = 70$ cm^{-1}) and high reorganization energies (0.8 and 0.4 eV, respectively). At the same time, if the frequency is such that one deals with quantum vibrations at low temperatures, the reaction continues up to the lowest temperatures. A correct description of the temperature behavior of reaction parameters requires an appropriate choice of quantum vibrational frequency. Earlier,[95—97] this choice was based on the temperature corresponding to the inflection point in the temperature dependence of the initial reaction rate (analogous plots for mutant RCs are available[68]); in this work, we were guided by the same considerations. The result exceeded our expectations since the model reproduces not only the temperature behavior of the initial reaction rate, but also the entire kinetic curves at all temperatures at which the reaction still proceeds.

As a concluding remark, mention may be made of the characteristic times of charge-transfer induced dielectric relaxation of proteins. The examples presented and the results obtained in this study confirm the existence of a broad spectrum of relaxation times characterizing the variety of relaxation processes in proteins. This should be taken into account in computer simulation of charge-transfer reactions because a typical trajectory in calculations of the dynamics of polyatomic systems is at most 10—100 ns long, which is insufficient to describe a slow rearrangement of the protein matrix in the course of charge redistribution in the active center of the enzyme (for more details, see Ref. 107).

Concluding Remarks

From this review it follows that studies of ETR in proteins are a rich source of data for constructing theoretical models to describe these processes and provide some ways of control of these reactions.

Interaction of forces and degrees of freedom of different nature on distances from a few Ångstrøms to a few nanometers in highly organized molecular systems leads to the onset of qualitatively different effects. It is biological macromolecular systems whose structure and functions have been polished to perfection during the evolution of life on the Earth that are very useful for complex analysis and research on such effects. This strategy of analysis of outworld phenomena appears to be very useful for both basic research and applied studies. This idea is quite obvious and has been discussed during the last two decades in numerous publications.[108—112] However, examples of detailed qualitative physicochemical analysis of the operation of real molecular devices are scarce.

Quantitative studies considered above show an important role of interactions of quantum and dynamic factors during electron transfer in a protein macromolecule built of a few thousands of atoms and having a size of a few nanometers. These are both quantum effects of tunneling over distances up to 1—2 nm and various relaxation processes due to quantum and mechanical degrees of freedom, which are realized locally or involve the entire protein globule. Variation of the contributions of different degrees of freedom significantly changes the electron transfer rate and allows one to effectively control the process.

Summing up the experience in the studies of long-range electron transfer reactions in RC and various metal-containing proteins, mention should be made of the following possible regularities of these processes:

1. Charge transfer in proteins occurs in a discrete fashion; electrons are localized on particular metal-containing complexes or clusters in the protein structure and transferred between them through tunneling over distances of the order of 0.5—2.5 nm with characteristic times from a few picoseconds to tens of milliseconds.

2. The kinetics of electron transfer between corresponding centers in proteins can be described within the framework of the theory of outer-sphere transfer provided that the structural and dynamic features of protein macromolecules are taken into account.

From the standpoint of directed long-range electron transfer, the most important feature of protein structures consists in optimum combination of quantum and mechanical factors. From the quantum standpoint, the chemical structure of the electron-transfer centers provides with the necessary redox potential and the possibility for the oxidation state to be changed fast and reversibly. These centers are separated by distances of 1—2 nm and superexchange interaction through the protein globule provides a weak overlap between their electron shells; nevertheless, it is strong enough to ensure electron tunneling with the desired velocity.

The second function of the protein globule consists in dielectric relaxation characterized by the optimum kinetic and energy parameters due to both quantum and classical degrees of freedom to provide efficient stabilization of separated charges in the course of charge transfer between the electron donor and acceptor centers. Thus, the protein is not only a static structure with fixed spatial localization of active centers. Activity of the protein structure involves some changes occurring in specified manner to provide with an optimum reaction trajectory in the phase space taking into account the quantum characteristics of the matrix. In other words, this is a molecular nanomachine whose activity to a great extent depends on the quantum effects. Fabrication of a molecular electronic device with specified function requires organization of centers with optimum redox properties (usually, they comprise one or more metal atoms and are of the order of a nanometer in size), their arrangement along the electron transfer chain at a distance of 1—2 nm from one another, and maintenance of the optimum dynamics of the environment.

Summing up, molecular devices for controlled charge transfer can not be very simple and small. They should be 5—10 nm in size (this is close to 10—100 atoms in diameter, see above[1]) and have a rather complex structure to provide relaxation along the degrees of freedom and allow one to effectively control them. At present, one can pose a problem of the design of molecular electronic devices based on, *e.g.*, biological macromolecules preliminarily modified in targeted manner by gene engineering methods to ensure their relative cheapness and possibility of large-scale production.

This work was financially supported by the Presidium of the Russian Academy of Sciences (Program No. 22, "Fundamentals of Basic Research on Nanotechnologies and Nanomaterials") and by the Russian Foundation for Basic Research (Project Nos 08-03-00094-a and 10-03-00687-a).

References

1. R. L. Feynman, *Ros. Khim. Zh.*, 2002, **5**, 4 [*Mendeleev Chem. J.* (*Engl. Transl.*), 2002, **5**].
2. K. M. C. Davis, D. D. Eley, R. S. Snart, *Nature*, 1960, **188**, 724.
3. A. Szent-Gyorgyi, *Int. J. Quant. Chem.: Quantum Biol. Symp.*, 1976, **3**, 45.
4. L. A. Blumenfeld, R. M. Davidov, *Biochem. Biophys. Acta*, 1979, **549**, 255.
5. S. L. Mayo, W. R. Ellis, R. J. Crutchley, H. B. Gray, *Science*, 1986, **233**, 948.
6. J. A. Cowan, R. K. Upmacis, D. N. Beratan, J. N. Onuchic, H. B. Gray, *Ann. N. Y. Acad. Sci.*, 1988, **550**, 68.

7. H. B. Gray, B. G. Malmström, *Biochemistry*, 1989, **28**, 7499.
8. O. Farver, I. Pecht, *Proc. Natl. Acad. Sci. USA*, 1989, **86**, 6968.
9. L. H. Zang, A. H. Maki, *J. Am. Chem. Soc.*, 1990, **112**, 4346.
10. D. N. Beratan, J. N. Onuchic, J. N. Betts, B. E. Bowler, H. B. Gray, *J. Am. Chem. Soc.*, 1990, **112**, 7915.
11. J. R. Winkler, H. B. Gray, *Chem. Rev.*, 1992, **92**, 369.
12. G. McLendon, R. Hake, *Chem. Rev.*, 1992, **92**, 481.
13. D. N. Beratan, J. N. Onuchic, J. R. Winkler, H. B. Gray, *Science*, 1992, **258**, 1740.
14. D. R. Casimiro, L. L. Wong, J. L. Colon, T. E. Zewert, J. H. Richards, I. J. Chang, J. R. Winkler, H. B. Gray, *J. Am. Chem. Soc.*, 1993, **115**, 1485.
15. D. R. Casimiro, J. H. Richards, J. R. Winkler, H. B. Gray, *J. Phys. Chem.*, 1993, **97**, 13073.
16. D. R. Casimiro, D. N. Beratan, J. N. Onuchic, J. R. Winkler, H. B. Gray, *Mechanistic Bioinorganic Chemistry*, Eds H. H. Thorp, V. Pecorado, Advances in Chemistry Series, American Chemical Society, Washington (DC), 1994, 134.
17. B. E. Ramirez, B. G. Malmström, J. R. Winkler, H. B. Gray, *Proc. Natl. Acad. Sci. USA*, 1995, **92**, 11949.
18. M. J. Bjerrum, D. R. Casimiro, I.-Yu. Chang, A. J. Di Billio, H. B. Gray, M. G. Hill, R. Langen, G. A. Mines, L. K. Skov, J. R. Winkler D. S. Wuttke, *J. Bioenergetics Biomembranes*, 1995, **27**, 295.
19. R. Langen, J. L. Colon, D. R. Casimiro, T. B. Karpishin, J. R. Wikler, H. B. Gray, *J. Biol. Inorg. Chem.*, 1996, **1**, 221.
20. T. Pascher, J. R. Winkler, H. B. Gray, *J. Am. Chem. Soc.*, 1998, **120**, 1102.
21. N. Liang, Ch. H. Kang, P. S. Ho, E. Margoliash, B. M. Hoffman, *J. Am. Chem. Soc.*, 1986, **108**, 4665.
22. M. J. Natan, B. M. Hoffman, *J. Am. Chem. Soc.*, 1989, **111**, 6468.
23. J. M. Nocek, N. Liang, S. A. Wallin, A. G. Mauk, B. M. Hoffman, *J. Am. Chem. Soc.*, 1990, **112**, 1623.
24. B. M. Hoffman, M. J. Natan, J. M. Nocek, S. A. Wallin, *Structure and Bonding*, Springer-Verlag, Berlin—Heidelberg, 1991, **75**, 85.
25. D. Kuila, W. W. Baxter, M. J. Natan, B. M. Hoffman, *J. Phys. Chem.*, 1991, **95**, 1.
26. L. A. Dick, I. Malfant, D. Kuila, S. Nebolsky, J. M. Nocek, B. M. Hoffman, M. A. Rather, *J. Am. Chem. Soc.*, 1998, **120**, 11401.
27. A. I. Berg, P. P. Noks, A. A. Kononenko, E. N. Frolov, N. Ya. Uspenskaya, I. N. Khrymova, A. B. Rubin, G. I. Likhtenshtein, V. I. Goldanskii, F. Parak, M. Bukl, R. Mössbauer, *Mol. Biologiya*, 1979, **13**, 81 [*Mol. Biol.* (*Engl. Transl.*), 1979, **13**, 81].
28. F. Parak, E. N. Frolov, A. A. Kononenko, R. L. Mössbauer, V. I. Goldanskii, A. B. Rubin, *FEBS Lett.*, 1980, **117**, 368.
29. D. Beece, L. Eisenstein, H. Frauenfelder, D. Good, M. C. Marden, L. Reinisch, A. H. Reynolds, L. B. Sorensen, K. T. Yue, *Biochemistry*, 1980, **19**, 5147.
30. G. I. Likhtenshtein, A. I. Kotelnikov, *Mol. Biologiya*, 1983, **17**, 505 [*Mol. Biol.* (*Engl. Transl.*), 1983, **17**].
31. A. I. Kotelnikov, V. R. Fogel´, V. V. Kochetkov, G. I. Likhtenshtein, P. P. Noks, N. P. Grishanova, A. A. Kononenko, A. B. Rubin, *Mol. Biologiya*, 1983, **17**, 846 [*Mol. Biol.* (*Engl. Transl.*), 1983, **17**].
32. V. V. Kochetkov, G. I. Likhtenshtein, V. K. Kol´tover, P. P. Noks, A. A. Kononenko, N. P. Grishanova, A. B. Rubin, *Izv. Akad. Nauk SSSR. Ser. Biol.*, 1984, **4**, 572 [*Bull. Acad. Sci. USSR*, *Biol.* (*Engl. Transl.*), 1984, **4**].
33. G. I. Likhtenstein, A. V. Kulikov, A. I. Kotelnikov, L. A. Levchenko, *J. Biochem. Biophys. Methods*, 1986, **12**, 1.
34. P. P. Noks, I. M. Bystryak, A. I. Kotelnikov, K. V. Shaitan, N. I. Zakharova, G. I. Likhtenshtein, A. B. Rubin, *Izv. Akad. Nauk SSSR. Ser. Biol.*, 1989, **5**, 651 [*Bull. Acad. Sci. USSR*, *Biol.* (*Engl. Transl.*), 1989, **5**].
35. J. S. Bashkin, G. McLendon, S. Mukamel, J. Marohn, *J. Phys. Chem.*, 1990, **94**, 4757.
36. T. Kitagawa, Y. Sakan, M. Nagai, T. Ogura, F. A. Fraunfelder, R. Mattera, M. Ikeda-Saito, *J. Inorg. Biochem.*, 1993, **51**, 217.
37. I-Yu. Chang, J. C. Lee, J. R. Winkler, H. B. Gray, *Proc. Natl. Acad. Sci. USA*, 2003, **100**, 3838.
38. T. Pascher, J. P. Chesick, J. R. Winkler, H. B. Gray, *Science*, 1996, **271**, 1558.
39. G. I. Likhtenshtein, S. M. Bystryak, A. I. Kotelnikov, *Khim. Fiz.*, 1990, **9**, 697 [*Chem. Phys.* (*Engl. Transl.*), 1990, **9**].
40. E. T. Rubtsova, V. R. Fogel´, D. V. Khudyakov, A. I. Kotelnikov, G. I. Likhtenshtein, *Biofizika*, 1993, **38**, 211 [*Biophysics* (*Engl. Transl.*), 1993, **38**].
41. V. R. Vogel, E. T. Rubtsova, G. I. Likhenshtein, K. Hideg, *J. Photochem. Photobiol. A: Chem.*, 1994, **83**, 229.
42. V. R. Vogel, A. V. Pastukhov, B. L. Psikha, A. I. Kotelnikov, *Biofizika*, 1997, **42**, 1008 [*Biophysics* (*Engl. Transl.*), 1997, **42**].
43. I. Chang, H. Hartmann, Yu. Krupyanskii, A. Zharikov, F. Parak, *Chem. Phys.*, 1996, **212**, 221.
44. Yu. F. Krupyanskii, V. I. Gol´danskii, *Usp. Fiz. Nauk*, 2002, **172**, 1247 [*Phys. Usp. (Engl. Transl.)*, 2002, **45**, 1131].
45. G. B. Postnikova, E. A. Shlyapnikova, B. P. Atanasov, M. V. Vol´kenshtein, *Mol. Biologiya*, 1982, **16**, 104 [*Mol. Biol.* (*Engl. Transl.*), 1982, **16**].
46. J. Deisenhofer, O. Epp, I. Sinning, H. Michel, *J. Mol. Biol.*, 1995, **246**, 429.
47. J. Hirst, *Biochem. J.*, 2010, **425**, 327.
48. G. L. Closs, J. R. Miller, *Science*, 1988, **240**, 440.
49. S. S. Isied, M. Y. Ogava, J. F. Wishart, *Chem. Rev.*, 1992, **92**, 381.
50. V. G. Levich, R. R. Dogonadze, *Dokl. Akad. Nauk SSSR*, 1959, **124**, 123 [*Dokl. Chem.* (*Engl. Transl.*), 1959].
51. R. A. Marcus, N. Sutin, *Biochem. Biophys. Acta*, 1985, **811**, 265.
52. D. De Vault, D. Chance, *Biophys. J.*, 1966, **6**, 825.
53. A. I. Kotelnikov, D.Sc. (Phys.-Math.) Thesis, M. V. Lomonosov Moscow State University, Moscow, 1991, 430 pp. (in Russian).
54. A. I. Kotelnikov, *Biofizika*, 1993, **38**, 217 [*Biophysics* (*Engl. Transl.*),1993, **38**].
55. C. C. Moser, J. M. Keske, K. Warncke, R. S. Farid, P. L. Dutton, *Nature*, 1992, **355**, 796.
56. A. I. Kotelnikov, V. R. Vogel, *Biofizika*, 1996, **41**, 596 [*Biophysics* (*Engl. Transl.*), 1996, **41**].
57. A. I. Kotelnikov, V. R. Vogel, A. V. Pastuchov, V. L. Voskoboinikov, E. S. Medvedev, in *Biological Electron Transfer Chains: Genetic, Composition and Mode of Operation. NATO ASI Series. Ser. C: Mathematical and Physical Sciences*, Eds G. W. Canters, E. Vijgenboom, Kluwer Academic Publishers, Dordrecht—Boston—London, 1998, **512**, 29.
58. P. Siddarh, R. A. Marcus, *J. Phys. Chem.*, 1993, **97**, 13078.
59. L. D. Zusman, *Chem. Phys.*, 1980, **49**, 295.

60. I. V. Alexandrov, *Chem. Phys.*, 1980, **51**, 449.
61. I. Rips, J. Jortner, *Chem. Phys. Lett.*, 1987, **133**, 411.
62. V. Z. Paschenko, S. S. Vasil´ev, V. V. Gorokhov, P. P. Knox, A. B. Rubin, in *Photosynthesis: From Light to Biosphere*, Ed. P. Mathis, Kluwer Academic Publishers, The Netherlands, 1995, **1**, 491.
63. V. Z. Paschenko, V. V. Gorokhov, N. P. Grishanova, E. A. Goryacheva, B. N. Korvatovsky, P. P. Knox, N. I. Zakharova, A. B. Rubin, *Biochim. Biophys. Acta*, 1998, **1364**, 361.
64. J. Gao, R. J. Shopes, C. A. Wraight, *Biochim. Biophys. Acta*, 1990, **1015**, 96.
65. J. M. Ortega, P. Mathis, *FEBS Lett.*, 1992, **301**, 45.
66. J. M. Ortega, P. Mathis, *Biochemistry*, 1993, **32**, 1141.
67. J. M. Ortega, B. Dohse, D. Oesterhelt, P. Mathis, *FEBS Lett.*, 1997, **401**, 153.
68. J. M. Ortega, B. Dohse, D. Oesterhelt, P. Mathis, *Biophys. J.*, 1998, **74**, 1135.
69. L. I. Krishtalik, *Biochim. Biophys. Acta*, 1996, **1273**, 139.
70. B. H. McMahon, J. D. Mûller, C. D. Wraight, G. U. Nienhaus, *Biophys. J.*, 1998, **74**, 2567.
71. J. M. Kriegl, F. K. Forster, G. U. Nienhaus, *Biophys. J.*, 2003, **85**, 1851.
72. J. M. Kriegl, G. U. Nienhaus, *Proc. Natl. Acad. Sci. USA*, 2004, **101**, 123.
73. E. N. Frolov, V. I. Goldanskii, A. Birk, F. Parak, *Eur. Biophys. J.*, 1996, **24**, 433.
74. A. I. Kotelnikov, J. M. Ortega, E. S. Medvedev, B. L. Psikha, D. Garsia, P. Mathis, *Elektrokhimiya*, 2001, **38**, 90 [*Russ. J. Electrochem.* (*Engl. Transl.*), 2001, **38**, 77].
75. A. I. Kotelnikov, J. M. Ortega, E. S. Medvedev, B. L. Psikha, D. Garsia, P. Mathis, *Bioelectrochem.*, 2002, **56**, 3.
76. A. I. Kotelnikov, N. S. Goryachev, A. Yu. Rubtsov, B. L. Psikha, J. M. Ortega, *Dokl. Akad. Nauk*, 2005, **405**, 830 [*Dokl. Biochem. Biophys.* (*Engl. Transl.*), 2005, **405**, 461].
77. E. S. Medvedev, A. I. Kotelnikov, N. S. Goryachev, B. L. Psikha, J. M. Ortega, A. A. Stuchebrukhov, *Molec. Simulat.*, 2006, **32**, 735.
78. E. S. Medvedev, A. I. Kotelnikov, A. V. Barinov, B. L. Psikha, J. M. Ortega, D. M. Popović, A. A. Stuchebrukhov, *J. Phys. Chem. B.*, 2008, **112**, 3208.
79. E. S. Medvedev, A. I. Kotelnikov, N. S. Goryachev, J. M. Ortega, A. A. Stuchebryukhov, *Khim. Fiz.*, 2011, **30**, 71 [*Russ. J. Phys. Chem. B* (*Engl. Transl.*), 2011, **5**, 308].
80. D. Holten, M. W. Windsor, W. W. Parson, J. P. Thornber, *Biochim. Biophys. Acta*, 1978, **501**, 112.
81. S. M. Dracheva, L. A. Drachev, A. A. Konstantinov, A. Yu. Semenov, V. P. Skulachev, A. M. Arutyunyan, V. A. Shuvalov, S. M. Zaberezhnaya, *Eur. J. Biochem.*, 1988, **171**, 253.
82. G. Venturoli, F. Drepper, J. C. Williams, J. P. Allen, X. Lin, P. Mathis, *Biophys. J.*, 1998, **74**, 3226.
83. R. J. Shopes, C. A. Wraight, *Biochim. Biophys. Acta*, 1987, **893**, 409.
84. H. Sumi, R. A. Marcus, *J. Chem. Phys.*, 1986, **84**, 4894.
85. D. W. Davidson, R. H. Cole, *J. Chem. Phys.*, 1951, **19**, 1484.
86. M. R. Gunner, B. Honig, *Proc. Natl. Acad. Sci. USA*, 1991, **88**, 9151.
87. M. Ya. Ovchinnikova, *Teor. Eksp. Khim.*, 1981, **17**, 651 [*Theor. Exp. Chem.* (*Engl. Transl.*), 1981, **17**].
88. O. Kaminskaya, A. A. Konstantinov, V. A. Shuvalov, *Biochim. Biophys. Acta*, 1990, **1016**, 153.
89. A. B. Helman, *Chem. Phys.*, 1982, **65**, 271.
90. A. B. Rubin, *Biofizika*, 3rd Ed., Nauka, Moscow, 2004, **1**, 462 pp. (in Russian).
91. A. B. Rubin, A. A. Kononenko, K. V. Shaitan, V. Z. Paschchenko, G. I. Riznichenko, *Biofizika*, 1994, **39**, 213 [*Biophysics* (*Engl. Transl.*), 1994, **39**].
92. J. Zhu, J. C. Rasaiah, *J. Chem. Phys.*, 1994, **101**, 9966.
93. E. Lee, E. S. Medvedev, A. A. Stuchebrukhov, *J. Chem. Phys.*, 2000, **112**, 9015.
94. A. M. Kuznetsov, *Charge Transfer in Physics, Chemistry, and Biology*, Gordon and Breach, Amsterdam, 1995.
95. J. J. Hopfield, *Proc. Natl. Acad. Sci. USA*, 1974, **71**, 3640.
96. J. Jortner, *J. Chem. Phys.*, 1976, **64**, 4860.
97. J. Jortner, *Biochim. Biophys. Acta*, 1980, **594**, 193.
98. B. Bagchi, G. R. Fleming, D. W. Oxtoby, *J. Chem. Phys.*, 1983, **78**, 7375.
99. C. C. Page, C. C. Moser, X. Chen, P. L. Dutton, *Nature*, 1999, **402**, 47.
100. A. A. Stuchebrukhov, *Theor. Chem. Acc.*, 2003, **110**, 291.
101. I.-P. Chen, P. Mathis, J. Koepke, H. Michel, *Biochemistry*, 2000, **39**, 3592.
102. D. A. Cherepanov, L. I. Krishtalik, A. Y. Mulkidjanian, *Biophys. J.*, 2001, **80**, 1033.
103. I. Muegge, P. X. Qi, A. J. Wand, Z. T. Chu, A. Warshel, *J. Phys. Chem. B.*, 1997, **101**, 825.
104. A. K. Churg, R. M. Weiss, A. Warshel, T. Takano, *J. Phys. Chem.*, 1983, **87**, 1683.
105. A. V. Barinov, N. S. Goryachev, A. I. Kotelnikov, *Opt. Spektrosk.*, 2011, **110**, 753 [*Opt. Spectrosc.* (*Engl. Transl.*), 2011, **110**, 724].
106. B. Dohse, P. Mathis, J. Wachtweitl, E. Laussermair, S. Iwata, H. Michel, D. Oesterhelt, *Biochemistry*, 1995, **34**, 11335.
107. I. V. Leontyev, A. A. Stuchebrukhov, *J. Chem. Phys.*, 2009, **130**, Article No. 085102.
108. K. E. Drexler, *Proc. Natl. Acad. Sci. USA*, 1981, **78**, 5275.
109. N. C. Seeman, *Nanotechnology*, 1991, **2**, 149.
110. K. E. Drexler, *Trends in Biotechnology*, 1999, **17**, 5.
111. R. C. Merkle, *Trends in Biotechnology*, 1999, **17**, 271.
112. P. Ball, *Nature*, 2001, **409**, 413.

Received March 4, 2011;
in revised form May 18, 2011